(NASA-CR-155533) A PRESSURIZED GAS SQUEEZE FILM JOURNAL DAMPER Final Report, 1 Jul. 1976 - Dec. 1977 (Mississippi State Univ., Mississippi State.) 89 p HC A05/MF A01 CSCI 13I G3/37

N78-15493

Unclas 55556

eirs
ENGINEERING & INDUSTRIAL RESEARCH STATION
MECHANICAL ENGINEERING – MISSISSIPPI STATE UNIVERSITY

A PRESSURIZED GAS SQUEEZE FILM JOURNAL DAMPER

by

A. KENT STIFFLER

MSSU-EIRS-ME-78-1

Final Report

COLLEGE OF ENGINEERING ADMINISTRATION

HARRY C. SIMRALL, M.S.
DEAN, COLLEGE OF ENGINEERING

WILLIE L. MCDANIEL, JR., PH.D.
ASSOCIATE DEAN

WALTER R. CARNES, PH.D.
ASSOCIATE DEAN

LAWRENCE J. HILL, M.S.
DIRECTOR, ENGINEERING EXTENSION

CHARLES B. CLIETT, M.S.
AEROPHYSICS & AEROSPACE ENGINEERING

WILLIAM R. FOX, PH.D.
AGRICULTURAL & BIOLOGICAL ENGINEERING

JOHN L. WEEKS, JR., PH.D.
CHEMICAL ENGINEERING

ROBERT M. SCHOLTES, PH.D.
CIVIL ENGINEERING

B. J. BALL, PH.D.
ELECTRICAL ENGINEERING

W. H. EUBANKS, M.ED.
ENGINEERING GRAPHICS

FRANK E. COTTON, JR., PH.D.
INDUSTRIAL ENGINEERING

C. T. CARLEY, PH.D.
MECHANICAL ENGINEERING

JOHN I. PAULK, PH.D.
NUCLEAR ENGINEERING

ELDRED W. HOUGH, PH.D.
PETROLEUM ENGINEERING

For additional copies or information
address correspondence to

ENGINEERING AND INDUSTRIAL RESEARCH STATION
DRAWER DE
MISSISSIPPI STATE UNIVERSITY
MISSISSIPPI STATE, MISSISSIPPI 39762

TELEPHONE (601) 325-2266

A PRESSURIZED GAS SQUEEZE FILM JOURNAL DAMPER

by

A. Kent Stiffler, Principal Investigator
Department of Mechanical Engineering

Supported by National Aeronautics and Space Administration
Grant NSG 3111

Mississippi State University
Engineering and Industrial Research Station
Mississippi State, MS 39762

Final Report

July 1, 1976 to December 1977

PREFACE

The report consists of two parts. Part I is a study of lumped parameter models and their ability to predict the stiffness and damping characteristics of gas film bearings and dampers. This effort was assisted by Shun-Lung Chao and represents his Master of Science thesis. Part II is an experimental investigation of the separation bubble near the inlet feeding region of inherently compensated gas bearings. Contributions to this work include Don Dye, a graduate student and Keith Logue, an undergraduate student in Mechanical Engineering.

PART I:

A LUMPED PARAMETER MODEL FOR GAS FILM BEARINGS

ABSTRACT

A lumped parameter model is developed to determine the stiffness and damping characteristics of inherently compensated gas film bearings. The model relies on the average static pressure over a one-dimensional strip bearing. Results of the model are compared with known computer solutions for the distributed strip and a two-dimensional square bearing. The results for the stiffness agree well with the computer solutions although the model proved to be inadequate for predicting the film damping.

TABLE OF CONTENTS

LIST OF FIGURES

LIST OF FIGURES (continued)

LIST OF APPENDIX TABLES

NOMENCLATURE

SYMBOL	DESCRIPTION
*	Denotes actual variable
o	Denotes average value
A_I	Area of the central region
A_p	Area of the bearing pad
C*	Damping
C	Dimensionless damping
C_D	Orifice discharge coefficient
D	d/dt^*
g_o	Gravitational acceleration
h*	Film thickness
h_o*	Average film thickness
h	Dimensionless film thickness (h^*/ h_o^*)
k	Ratio of Specific heats (C_p/C_v)
K_s*	Stiffness
K_s	Dimensionless Stiffness
L*	Bearing width
M_I*	Mass flow to the central region
M_{II}*	Mass flow through sill region
M_r*	Mass flow through the inlets
M_{in}*	Mass flow into the bearing pad
M_{out}*	Mass flow out of the bearing pad
m_o*	Average mass flow

NOMENCLATURE (continued)

SYMBOL	DESCRIPTION
P^*	Pressure
P_a^*	Ambient pressure
P	Dimensionless pressure (P^*/P_a^*)
P_r	Dimensionless pressure downstream of inlet
P_{ro}	Dimensionless average pressure downstream of inlet
P_s	Supply pressure
P_{II}	Average pressure across the sill region
r	Inlet span to total bearing span ratio
R	Gas constant
Sd^*	Dynamic stiffness ($-\Delta W^*/\Delta h^*$)
t^*	Time
t	Dimensionless time ($t^*\Omega^*$)
T	Gas temperature
V_I	Film volume of the central region
V_{II}	Film volume of the sill region
w^*	Bearing width
W^*	Total bearing load capacity
W	Dimensionless bearing load
$\overline{W}$	Average bearing load
X^*, Z^*	Cartesian coordinate
ρ^*	Gas density
ρ_I^*	Film density of the central region

NOMENCLATURE (continued)

SYMBOL	DESCRIPTION
ρ_{II}^*	Film density of the sill region
μ	Gas viscosity
σ	Squeeze Number
Ω^*	Excitation frequency
Λ	Restrictor coefficient
λ	Ratio of the central area to the bearing area (A_I/A_p)
ε	Amplitude of disturbance

CHAPTER I

INTRODUCTION

The range of application for externally pressurized gas lubricated bearings has been increasing steadily in recent years. The reason for this trend is the many advantages of gas lubrication. Gas bearings offer extremely low friction due to the low viscosity of the gas; so mechanical efficiency is high, but heat generation is low, especially in low or medium speed rotation. Because of the absence of metal-to-metal contact which promises freedom from wear, the life of the bearing is long. Also, gas bearings provide silent and vibrationless running and are able to operate in extremely high or low temperature. In addition, because of the distributing action of the gas film, gas bearings can reduce the effect of local errors of geometry and produce an accurate mode of motion. According to these advantages, gas bearings have been successfully applied in increasing amounts in many industrial applications over the past few years.

Although gas lubrication offered many advantages, two major problems exist:

(1) the existence of a self-excited film whirl instability [1]* in which machines can not be run in excess of the whirl onset speed;

(2) the limitation of the bearing load capacity which usually results in severe damage to the bearing surfaces by overloading.

---

*Numbers in brackets refer to REFERENCES.

The response of gas bearings is affected by the dynamic characteristics of the lubricating film. To study this problem, the gas film can be approximated as a linear spring-dashpot system subjected to a small amplitude, periodic load disturbance. Thus, stiffness and damping are important parameters describing the dynamic response of this system. In order to determine the dynamic bearing load, the Reynolds' equation must be solved for the pressure distribution in the gas film. The Reynolds' equation is a nonlinear, time-dependent,parabolic, partial differential equation; so it is difficult to find exact solutions for this equation. For obtaining approximate solutions, small-perturbation theory is often combined with finite-difference methods. Limited use has been made of so called " lumped parameter" methods, but their accuracy is not clearly understood. A review of the literature discussing the above methods will now be given.

1.1 Review of literature

Richardson[2] analyzed the static and dynamic performance of gas bearings based on lumped parameter methods. He derived the relationships of the bearing parameters to be used for design information. Licht and Elrod[3] studied the stability of externally pressurized gas bearings using distributed parameter methods. Their results when compared with those obtained by Richardson using lumped parameter methods showed a marked divergence among the limiting values of parameters which affect the stability of the bearing. Stiffler[4] used distributed parameter methods to study an inherently compensated, multiple-inlet, circular thrust bearing. In his analysis, the

Reynolds' equation was solved by small-perturbation theory, and the results were given for the bearing coefficients (stiffness and damping) as functions of inlet location, excitation frequency, supply pressure, and restrictor coefficient. Mullan and Richardson[5] used lumped and distributed parameter methods to develop the dynamic characteristics of an inherently compensated gas journal bearing and compared the analysis with experiment.

Lund [6] carried out a theoretical analysis of the load-carrying capacity of the hydrostatic gas journal bearing with journal rotation and vibration. Results were obtained from a first-order perturbation solution by assuming small eccentricity ratio and small vibration amplitude. Also, Lund [7] analyzed the threshhold of instability for a rigid rotor supported in pressurized gas journal bearing based on a first-order pertubation with respect to the eccentricity ratio and makes use of the "linearized Ph" methods. Numerical results are given as a function of supply pressure ratio, feeding parameter, and eccentricity ratio.

Stiffler and Smith [8] analyzed the dynamic characteristics of an inherently compensated, square gas film bearing using small perturbations of the Reynolds' equation. They obtained the results by finite-difference methods and presented the design curves for the load capacity, mass flow, stiffness and damping as a function of squeeze number, supply pressure, restrictor coefficient, and inlet location. Stiffler and Tapia [9] presented a theoretical analysis of the amplitude effects on the dynamic characteristics of an inherently, compensated, infinitively long strip, gas thrust bearing.

Squeeze number (dimensionless frequency) is an important parameter in understanding the dynamic response. Sadd and Stiffler [10] analyzed gaseous squeeze film dampers at low squeeze numbers and determined the effect of periodic disturbance amplitude on the dynamic performance. The results are useful in predicting the behavior of externally pressurized gas bearings under certain conditions. Earlier, working with circular squeeze films, Salbu [11] presented computer solutions of the pressure distribution as a function of the squeeze number. A superambient average film pressure was introduced by compressibility effects at high squeeze numbers, so that a gas film can support a load while operating on squeeze effects only. These results were supported by experiment.

1.2 Statement of the Problem

The general problem of obtaining the dynamic characteristics of externally pressurized, inherently compensated, gas thrust bearings is the solution of the Reynolds' equation, a non-linear partial differential equation in space and time. Solutions of this equation by finite-difference techniques have presented difficulties in the past, particularly related to convergence time. Furthermore, the multitude of parameters have limited the amount of information that can be received from the computer and illustrated for the designer. The purpose of this thesis is to develop a lumped parameter model for these bearings in analytical form. Such a model can provide a quick, though approximate solution for the designer as well as provide a check on the more accurate finite-difference solution if it is so

desired.

The following chapter on analytical methods contains two sections : (1) a finite-difference solution of the strip bearing, Figure 1, which has been condensed from REFERENCE [9]; (2) a general lumped parameter model for all bearings. The solution of the strip is outlined here for several reasons: (1) parallels can be observed between the two methods; (2) many of the basic equations are pertinent to both methods, including dimensionless parameters; (3) lumped solutions of more complicated two-dimensional bearings can be inferred from a model of the strip which includes aspects of the exact solution; (4) comparisons between two solutions can give some insight into the accuracy of the lumped model.

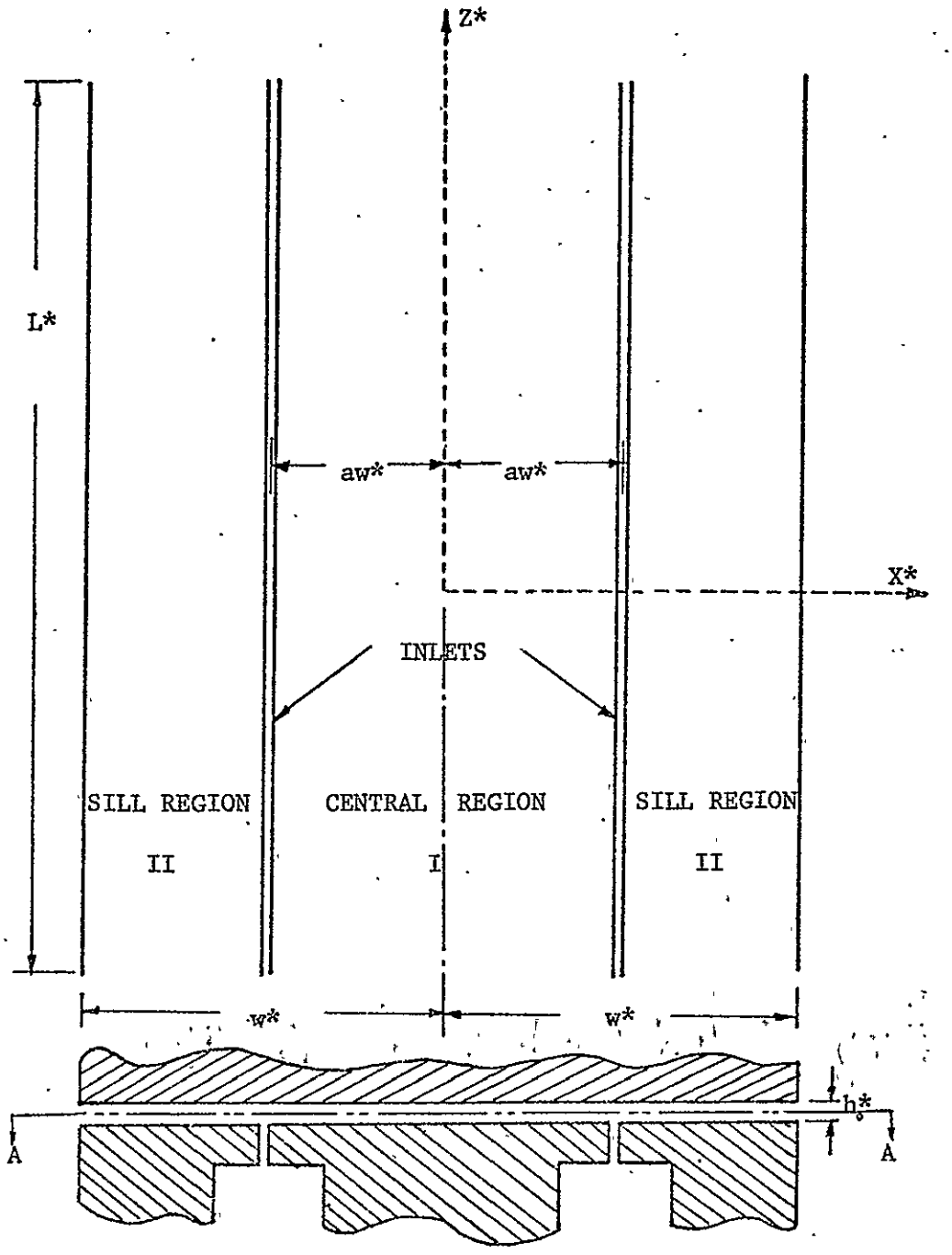

FIGURE 1. Inherently Compensated, Long Strip, Thrust Bearing

CHAPTER II

ANALYSIS OF AN INHERENTLY COMPENSATED STRIP THRUST BEARING

2.1 The Strip Bearing (Condensed from REFERENCE [9])

To develop the theoretical analysis of the strip bearing, it is divided into two different regions (Figure 1): the central region or region I, and the sill region or region II. In order to simplify the problem, only one-half of the strip bearing is considered because the geometry is symmetric about the centerline. Furthermore, the inlets are assumed to be sufficient in number so that they may be considered as an inherently equivalent line source. It is also assumed that the length of the strip bearing in the Z-axis is infinite.

2.1.1. Reynolds' Equation

Before solving for the bearing mass flow, bearing load capacity, bearing stiffness, and bearing damping, the pressure distribution across the bearing first has to be determined. The pressure distribution in the clearance of an externally pressurized bearing is governed by the Reynolds' equation [12];

$$\frac{\partial}{\partial x^*}\left(h^{*3} \rho^* \frac{\partial P^*}{\partial x^*} \right) + \frac{\partial}{\partial z^*}\left(h^{*3} \rho^* \frac{\partial P^*}{\partial z^*} \right) = 12\mu \frac{\partial}{\partial t^*}(\rho^* h^*) \quad (2\text{-}1a)$$

where the starred symbols denote real variables. Since two surfaces of the bearing are parallel and rigid, the film thickness, h^*, is uniform across the bearing.

For the strip bearing, the pressure distribution is described by

the reduced Reynolds' equation:

$$\frac{\partial}{\partial x^*}\left(h^{*3} \rho^* \frac{\partial p^*}{\partial x^*}\right) = 12\mu \frac{\partial}{\partial t^*}\left(\rho^* h^*\right) \qquad (2\text{-}1b)$$

In order to simplify the analysis, the film is assumed to behave as an ideal gas with constant specific heats. It is also assumed that the flow is isothermal with P^*/ρ^*=constant.

To solve equation (2-1a), the following nondimensional variables are introduced:

$$x = x^* / w^* \qquad (2\text{-}2a)$$

$$h = h^*/h_o^* \qquad (2\text{-}2b)$$

$$P = P^*/P_a^* \qquad (2\text{-}2c)$$

$$t = t^*\Omega^*$$

Thus, equation (2-1b) can be written as

$$\frac{\partial^2}{\partial x^2}\left(P^2\right) = \frac{2\sigma}{h^3} \frac{\partial}{\partial t}(Ph) \qquad (2\text{-}3)$$

where the squeeze number, σ, is defined as

$$\sigma = \frac{12\mu \Omega^* w^{*2}}{h_o^{*2} P_a^*} \qquad (2\text{-}4)$$

and the subscript symbol, o, denotes average condition. The film thickness, h, is a function of time because it depends on the load disturbance.

To solve equation (2-3), the boundary conditions must be known. The average pressure downstream of inlets is given by P_{ro}, and the pressure at the edges of the sill region is ambient. Thus, the boundary conditions, which are normalized by the ambient pressure

are

$$P = P_{ro} \qquad \text{at } x = a \tag{2-5a}$$

$$P = 1 \qquad \text{at } x = 1 \tag{2-5b}$$

Applying equations (2-5a) and (2-5b) to equation (2-3), the average pressure distribution through the bearing can be determined as

$$P = P_{ro} \qquad 0 \leq x \leq a \tag{2-6a}$$

$$P = \left[1+\left(\frac{P_{ro}^2-1}{1-a}\right)(1-x)\right]^{1/2} \qquad a \leq x \leq 1 \tag{2-6b}$$

where 'a' is the dimensionless distance from the centerline to the inlets.

2.1.2. Mass Flow

From the continuity condition at the inlets, the following relation has to be met:

$$M_r^* + M_I^* = M_{II}^* \tag{2-7}$$

where

M_r^* = mass flow through the inlets

M_I^* = mass flow through the central region

M_{II}^*= mass flow through the sill region

The mass flow across two parallel, long strips is given by Constantinescu [12] as

$$M_x^* = -\int_0^{L^*} \rho^* \frac{h^{*3}}{12\mu} \frac{\partial P^*}{\partial x^*} \, dz^* \tag{2-8}$$

Since the flow is isothermal, equation (2-8) becomes

$$M_x^* = -\frac{L^* h^{*3} P_a^{*2}}{24\mu RTw^*} \frac{\partial}{\partial x}(P^2) \tag{2-9}$$

Thus, the average mass flow through the central region and the sill region can be determined from equation (2-9) by applying equations (2-6a) and (2-6b) to obtain

$$M_I^* = 0 \tag{2-10}$$

and

$$M_{II}^* = 2M_x^* = \frac{L^* h^{*3} P_a^{*2}}{12\mu RTw^*} \frac{(Pr^2 - 1)}{(1 - a)} \tag{2-11}$$

The mass flow through the inlets [13] is described by

$$M_r^* = \frac{2C_D L^* h^* P_a^* P_s}{(RT)^{1/2}} \left(\frac{2g_o k}{k-1}\right)^{1/2} \left(\frac{P_r}{P_s}\right)^{\frac{1}{k}} \left[1 - \left(\frac{P_r}{P_s}\right)^{\frac{k-1}{k}}\right]^{1/2}$$

$$\frac{P_r}{P_s} > \left(\frac{2}{k+1}\right)^{\frac{k}{k-1}} \tag{2-12}$$

or

$$M_r^* = \frac{2C_D L^* h^* \rho_a^* P_s}{(RT)^{\frac{1}{2}}} \left(\frac{2g_o k}{k-1}\right)^{\frac{1}{2}} \left(\frac{2}{k+1}\right)^{\frac{1}{k-1}}$$

$$\frac{P_r}{P_s} \leq \left(\frac{2}{k+1}\right)^{\frac{k}{k-1}} \qquad (2\text{-}13)$$

Since the average mass flow through the inlet and the sill are the same, the average pressure downstream of the orifice, P_{ro}, is established by

$$1 = \frac{\wedge}{(P_{ro}^2 - 1)} \left(\frac{P_{ro}}{P_s}\right)^{\frac{1}{k}} P_s^2 \left[1 - \left(\frac{P_{ro}}{P_s}\right)^{\frac{k-1}{k}}\right]^{\frac{1}{2}}$$

$$\frac{P_{ro}}{P_s} > \left(\frac{2}{k+1}\right)^{\frac{k}{k-1}} \qquad (2\text{-}14)$$

or

$$P_{ro}^2 = 1 + \wedge P_s^2 \left(\frac{k-1}{k+1}\right)^{\frac{1}{2}} \left(\frac{2}{k+1}\right)^{\frac{1}{k-1}}$$

$$\frac{P_{ro}}{P_s} \leq \left(\frac{2}{k+1}\right)^{\frac{k}{k-1}} \qquad (2\text{-}15)$$

where the restictor coefficient, Λ, is defined by

$$\Lambda = \frac{24 C_{D/\!/} w^* (1-a)}{P_s P_a^* h_o^{*2}} \left(\frac{2 g_o k R T}{k-1} \right)^{\frac{1}{2}} \tag{2-16}$$

The restrictor coefficient, Λ, is a nondimensional parameter which indicates the ratio of the resistance of the mass flow through the sill region to the mass flow resistance across the inlets. For critical flow, P_{ro} is obtained directly from equation (2-15). But for subcritical flow, P_{ro} is solved by the Newton-Raphson method (see APPENDIX for tables relating P_{ro} to Λ) since equation (2-14) is implicit for P_{ro}. After P_{ro} is known, the pressure distribution, equations (2-6a) and (2-6b), can be determined.

2.1.3 Bearing Load Capacity

The bearing load capacity is given by

$$\begin{aligned} W^* &= 2\int_o^{w^*} (P^* - P_a^*)\, L^* dx^* \\ &= 2 w^* L^* P_a^* \int_o^1 (P-1)\, dx \end{aligned} \tag{2-17}$$

where the pressure P is attained from the reduced Reynolds' equation (2-3). Thus, the dimensionless load capacity is derived from equation (2-17) as

$$W = \frac{W^*}{2 w^* L^* P_a^*} = \int_o^1 (P - 1)\, dx \tag{2-18}$$

Substituting equations (2-6a) and (2-6b) into equation (2-18), the average load capacity is obtained as

$$\bar{W} = a(P_r - 1) + \left[\frac{2}{3}\left(\frac{P_r^3 - 1}{P_r^2 - 1}\right) - 1\right](1 - a) \tag{2-19}$$

Thus, the average pressure across the sill region can be found from equation (2-19) as

$$P_{II} = \frac{2}{3}\left(\frac{P_r^3 - 1}{P_r^2 - 1}\right) \tag{2-20}$$

2.2 Lumped Parameter Model

Since the gas film behaves as a simple, linear, first order system for small disturbance amplitudes, the load changes, which are usually periodic in nature, exhibit components in phase and ninety degrees out of phase with displacement. Thus, a dynamic stiffness is defined as

$$S_d^* = -\frac{\Delta W^*}{\Delta h^*}$$

$$= -\frac{\Delta W^*}{\Delta P_r^*}\left[\frac{\Delta P_r^*}{\Delta h^*}\right] \tag{2-21}$$

The bearing load capacity is a function of the pressure downstream of the inlets only, so

$$\frac{\Delta W^*}{\Delta P_r^*} = 2w^*L^* \frac{d\bar{W}}{dP_r} \tag{2-22}$$

where the bearing load capacity is given by equation (2-19).

The conservation of mass flow requires that the net mass flow into the bearing pad is equal to the change of mass stored in the bearing pad. Thus,

$$M_{in}^* - M_{out}^* = \frac{d}{dt^*} (\text{mass})_{pad}$$

$$= \frac{d}{dt^*} (\rho^* V)_{\text{central region}} + \frac{d}{dt^*} (\rho^* V)_{\text{sill region}}$$

$$= D(\rho_I^* V_I) + D(\rho_{II}^* V_{II}) \tag{2-23}$$

where

$$D = \frac{d}{dt^*}$$

ρ_I^* = film density of the central region $= \rho_r^*$

V_I = film volume of the central region

ρ_{II}^* = film density of the sill region

V_{II} = film volume of the sill region

Linearizing equation (2-23) for small changes from the steady-state conditions, equation (2-23) becomes

$$\Delta M_{in}^* - \Delta M_{out}^* = [\rho_{Io}^* D(V_I) + V_{Io} D(\rho_I^*)] + [\rho_{II_o}^* D(V_{II}) + V_{II_o} D(\rho_{II}^*)] \tag{2-24}$$

where the symbol, o, denotes average condition. Also, the following relations are introduced:

$$P_r^* = P_{ro}^* + \Delta P_r^* \tag{2-25a}$$

$$h^* = h_o^* + \Delta h^* \tag{2-25b}$$

$$\lambda = A_I/A_p \tag{2-25c}$$

where A_I and A_p are the area of the central region and the total bearing pad respectively.

Since the average pressure across the sill region is found from equation (2-20), the following relations are derived.

$$\rho_{Io}^* = \left(\frac{P_a^*}{RT}\right) P_{ro} \tag{2-26a}$$

$$D(V_I) = \lambda A_p D(\Delta h^*) \tag{2-26b}$$

$$V_{Io} = \lambda A_p h_o^* \tag{2-26c}$$

$$D(\rho_I^*) = \left(\frac{1}{RT}\right) D(\Delta P_r^*) \tag{2-26d}$$

$$\rho_{IIo}^* = \frac{2}{3}\left(\frac{P_a^*}{RT}\right)\left(\frac{P_{ro}^3 - 1}{P_{ro}^2 - 1}\right) \tag{2-26e}$$

$$D(V_{II}) = (1-\lambda)\, A_p\, D(\Delta h^*) \tag{2-26f}$$

$$V_{IIo} = (1-\lambda)\, A_p h_o^* \tag{2-26g}$$

$$D(\rho_{II}^*) = \frac{2}{3}\left(\frac{1}{RT}\right)\left[\frac{P_{ro}(P_{ro}^3 - 3P_{ro} + 2)}{(P_{ro}^2 - 1)^2}\right] D\,(\Delta P_r^*) \tag{2-26h}$$

The mass flow into and out of the bearing pad is a function of film thickness and the pressure downstream of the inlets. Thus, the following relations can be found:

$$\Delta M_{in}^* = \left(\frac{\partial M_{in}^*}{\partial h^*}\right)\Delta h^* + \left(\frac{\partial M_{in}^*}{\partial P_r^*}\right)\Delta P_r^* \tag{2-27a}$$

$$\Delta M_{out}^* = \left(\frac{\partial M_{out}^*}{\partial h^*}\right)\Delta h^* + \left(\frac{\partial M_{out}^*}{\partial P_r^*}\right)\Delta P_r^* \tag{2-27b}$$

Substituting equation (2-26) and (2-27) into equation (2-24), the following relation is obtained:

$$\frac{\Delta P_r^*}{\Delta h^*} = \frac{\dfrac{A_p P_a^*}{RT}\left[\lambda P_{ro} + \dfrac{2}{3}(1-\lambda)\dfrac{P_{ro}^3 - 1}{P_{ro}^2 - 1}\right] D + \left(\dfrac{\partial M_{out}^*}{\partial h^*} - \dfrac{\partial M_{in}^*}{\partial h^*}\right)}{-\dfrac{A_p h_o^*}{RT}\left[\lambda + \dfrac{2}{3}(1-\lambda)\left[\dfrac{P_{ro}(P_{ro}^3 - 3P_{ro} + 2)}{(P_{ro}^2 - 1)^2}\right]\right] D + \left(\dfrac{\partial M_{out}^*}{\partial P_r^*} - \dfrac{\partial M_{in}^*}{\partial P_r^*}\right)} \tag{2-28}$$

Equations (2-22) and (2-28) are introduced into equation (2-21), then

$$S_d^* = k_s^*\left(\frac{\tau_1 D + 1}{\tau_2 D + 1}\right) \tag{2-29}$$

where

$$k_s^* = \frac{dW^*}{dP_r^*}\left(\frac{\frac{\partial M_{out}^*}{\partial h^*} - \frac{\partial M_{in}^*}{\partial h^*}}{\frac{\partial M_{out}^*}{\partial P_r^*} - \frac{\partial M_{in}^*}{\partial P_r^*}}\right) \tag{2-30}$$

$$\tau_1 = \frac{\frac{A_p P_a^*}{RT}\left[\lambda P_{ro} + \frac{2}{3}(1-\lambda)\left(\frac{P_{ro}^3 - 1}{P_{ro}^2 - 1}\right)\right]}{\frac{\partial M_{out}^*}{\partial h^*} - \frac{\partial M_{in}^*}{\partial h^*}} \tag{2-31}$$

$$\tau_2 = \frac{\frac{A_p h_o^*}{RT}\left\{\lambda + \frac{2}{3}(1-\lambda)\left[\frac{P_{ro}(P_{ro}^3 - 3P_{ro} + 2)}{(P_{ro}^2 - 1)^2}\right]\right\}}{\frac{\partial M_{out}^*}{\partial P_r^*} - \frac{\partial M_{in}^*}{\partial P_r^*}} \tag{2-32}$$

A linear approximation of the bearing motion is

$$\Delta W^* = -K_s^* \Delta h^* - C^* D\left[\Delta h^*\right] \tag{2-33}$$

Thus,

$$S_d^* = K_s^* + C^* D \tag{2-34}$$

where K_s^* and C^* represent the stiffness and damping of the bearing respectively.

For a periodic load disturbance, the D operator in equations (2-29) and (2-34) can be replaced by $j\Omega^*$ operator. Then,

$$Sd^* = k_s^* \left[\frac{(1 + \Omega^{*2} \tau_1 \tau_2) + (\tau_1 - \tau_2)\, j\Omega^*}{1 + \Omega^{*2} \tau_2^{\,2}} \right] \tag{2-35}$$

$$Sd^* = K_s^* + C^* j\Omega^* \tag{2-36}$$

From equations (2-35) and (2-36), the stiffness and damping can be determined as

$$K_s^* = \frac{k_s^* \,(1 + \Omega^{*2} \tau_1 \tau_2)}{(1 + \Omega^{*2} \tau_2^{\,2})} \tag{2-37}$$

$$C^* = \frac{k_s^* \,(\tau_1 - \tau_2)}{1 + \Omega^{*2} \tau_2^{\,2}} \tag{2-38}$$

For certain conditions, equations(2-37) and (2-38) reduce to the following:

$$K_s^* = k_s^*$$

$$\text{when } \Omega^* \ll \frac{1}{\sqrt{\tau_1 \tau_2}} \quad \text{and } \Omega^* \ll \frac{1}{\tau_2} \tag{2-39}$$

$$K_s^* = \frac{\tau_1 k_s^*}{\tau_2}$$

$$\text{when } \Omega^* \gg \sqrt{\frac{1}{\tau_1 \tau_2}} \text{ and } \Omega^* \gg \frac{1}{\tau_2} \tag{2-40}$$

$$C^* = k_s^* (\tau_1 - \tau_2)$$

$$\text{when } \Omega^* \ll \frac{1}{\tau_2} \tag{2-41}$$

The nondimensional stiffness and damping are defined by [9]

$$K_s = \frac{K_s^* h_o^*}{2w^* L^* P_a^* (P_s - 1)} \tag{2-42a}$$

$$= \frac{k_s^* h_o^*}{2w^* L^* P_a^* (P_s - 1)} \tag{2-42b}$$

$$C = \frac{C^*}{2\mu L^* \left(\frac{w^*}{h_o^*}\right)^3} \tag{2-43a}$$

$$= \frac{k_s^* (\tau_1 - \tau_2)}{2\mu L^* \left(\frac{w^*}{h_o^*}\right)^3} \tag{2-43b}$$

From equations (2-10), (2-11), (2-13), and (2-19), the following relations can be obtained:

$$\left.\frac{dW^*}{dP_r^*}\right|_{P_{ro}} = 2w^* L^* \left\{ a + \frac{2(1-a)}{3} \left(\frac{P_{ro}}{P_{ro}^2 - 1} \right) \left[3P_{ro} - \frac{2(P_{ro}^3 - 1)}{(P_{ro}^2 - 1)} \right] \right\} \tag{2-44}$$

$$\left.\frac{\partial M_{out}^*}{\partial h^*}\right|_{h_o^*,\ P_{ro}} = 3\left(\frac{m_o^*}{h_o^*}\right) \tag{2-45}$$

$$\left.\frac{\partial M_{out}^*}{\partial P_r^*}\right|_{h_o^*,\ P_{ro}} = 2\left\{\frac{P_{ro} m_o^*}{P_a^*(P_{ro}^2 - 1)}\right\} \tag{2-46}$$

where $$m_o^* = \frac{L^* P_a^{*2} h_o^{*3}}{\mu RT\ w^*}\ m_o \tag{2-47}$$

$$m_o = \frac{(P_{ro}^2 - 1)}{12(1 - a)} \tag{2-48}$$

and

$$\left.\frac{\partial M_{in}^*}{\partial h^*}\right|_{h_o^*,\ P_{ro}} = \frac{m_o^*}{h_o^*} \tag{2-49}$$

$$\left.\frac{\partial M_{in}^*}{\partial P_r^*}\right|_{h_o^*,\ P_{ro}} = \left\{\frac{1}{P_{ro}} - \left(\frac{P_s}{P_{ro}}\right)^{\frac{1}{k}} \frac{(k-1)}{2P_s\left\{1-\left(\frac{P_{ro}}{P_s}\right)^{\frac{k-1}{k}}\right\}}\right\} \frac{m_o^*}{kP_a^*} \tag{2-50}$$

where

$$\frac{P_{ro}}{P_s} > \left(\frac{2}{k+1}\right)^{\frac{k}{k-1}}$$

or

$$\left.\frac{\partial M_{in}^*}{\partial h^*}\right|_{h_o^*,P_{ro}} = \frac{m_o^*}{h_o^*} \tag{2-51}$$

$$\left.\frac{\partial M_{in}^{*}}{\partial P_r^{*}}\right|_{h_o^{*},P_{ro}} = 0 \qquad (2\text{-}52)$$

when

$$\frac{P_{ro}}{P_s} \leq \left(\frac{2}{k+1}\right)^{\frac{k}{k-1}}$$

Substituting the above relations into equations (2-42) and (2-43), the nondimensional stiffness and damping can be found:

$$K_s = \left(\frac{P_{ro}^{2}-1}{P_s-1}\right)\frac{\lambda + \frac{2(1-\lambda)}{3}\left(\frac{P_{ro}}{P_{ro}^{2}-1}\right)\left\{3P_{ro} - \frac{2(P_{ro}^{3}-1)}{(P_{ro}^{2}-1)}\right\}}{P_{ro} - \left(\frac{P_{ro}^{2}-1}{2kP_{ro}}\right)\left\{1 - \left(\frac{P_{ro}}{P_s}\right)^{\frac{k-1}{k}}\frac{(k-1)}{2\left[1-\left(\frac{P_{ro}}{P_s}\right)^{\frac{k-1}{k}}\right]}\right\}} \qquad (2\text{-}53)$$

$$C = \frac{K_s(P_s-1)}{m_o}\left\{\lambda P_{ro} + \frac{2}{3}(1-\lambda)\left(\frac{P_{ro}^{3}-1}{P_{ro}^{2}-1}\right) - \frac{2\left\{\lambda + \frac{2}{3}(1-\lambda)\,P_{ro}\,\frac{(P_{ro}^{3}-3P_{ro}+2)}{(P_{ro}^{2}-1)^{2}}\right\}}{\left(\frac{2P_{ro}}{P_{ro}^{2}-1}\right) - \frac{1}{k}\left\{\frac{1}{P_{ro}} - \left(\frac{P_s}{P_{ro}}\right)^{\frac{1}{k}}\frac{(k-1)}{2P_s\left[1-\left(\frac{P_{ro}}{P_s}\right)^{\frac{k-1}{k}}\right]}\right\}}\right\} \qquad (2\text{-}54)$$

when $\frac{P_{ro}}{P_s} > \left(\frac{2}{k+1}\right)^{\frac{k}{k-1}}$

or

$$K_s = \left(\frac{P_{ro}^2 - 1}{P_s - 1}\right)\left\{\frac{\lambda}{P_{ro}} + \frac{2(1-\lambda)}{3}\,\frac{1}{(P_{ro} - 1)}\left[3P_{ro} - \frac{2(P_{ro}^3 - 1)}{(P_{ro}^2 - 1)}\right]\right\} \quad (2\text{-}55)$$

$$C = \frac{K_s(P_s - 1)}{m_o}\left\{\lambda P_{ro} + \frac{2}{3}(1-\lambda)\left(\frac{P_{ro}^3 - 1}{P_{ro}^2 - 1}\right) - \left(\frac{P_{ro}^2 - 1}{P_{ro}}\right)\right.$$

$$\left.\cdot\left[\lambda + \frac{2}{3}(1-\lambda)\,P_{ro}\,\frac{(P_{ro}^3 - 3P_{ro} + 2)}{(P_{ro}^2 - 1)^2}\right]\right\} \quad (2\text{-}56)$$

when

$$\frac{P_{ro}}{P_s} \leq \left(\frac{2}{k+1}\right)^{\frac{k}{k-1}}$$

Thus, after the inlet location, supply pressure, average pressure downstream of the inlets are known, the dimensionless stiffness and damping can be found from equations (2-53), (2-54), (2-55), and (2-56).

CHAPTER III

RESULTS AND MODEL COMPARISONS FOR THE STRIP BEARING

The stiffness and damping are obtained in this study as functions of restrictor coefficient and the supply pressure with inlet location (a=0.5 in this study) fixed. They are compared with computer solutions by Stiffler and Tapia [9] at low amplitude of disturbance (ε=0.1) and small squeeze number (σ=0.1). The amplitude effect on the stiffness and damping can be neglected at low amplitude of disturbance. The stiffness and damping are insensitive to small squeeze numbers (σ<.4), but the stiffness increases and the damping decreases when the squeeze number exceeds this value [9]. Design curves for the stiffness and damping are discussed and compared below for the lumped parameter approach and the computer solutions.

3.1 Stiffness

The dimensionless stiffness is a function of the restrictor coefficient, Λ, and supply pressure as shown in the Figures 2-6. The stiffness is very sensitive to the restrictor coefficient. When the restrictor coefficient becomes small, the stiffness approaches zero. The stiffness reaches the maximum in the range $1.3<\Lambda<2.2$ where the mass flow through the inlets is critical. As the restrictor coefficient becomes large, the stiffness approaches zero again.

If the stiffness is compared with computer solutions by Stiffler and Tapia [9] as shown in Figures2-6, it can be observed that the results of the lumped model agree well with computer solutions.

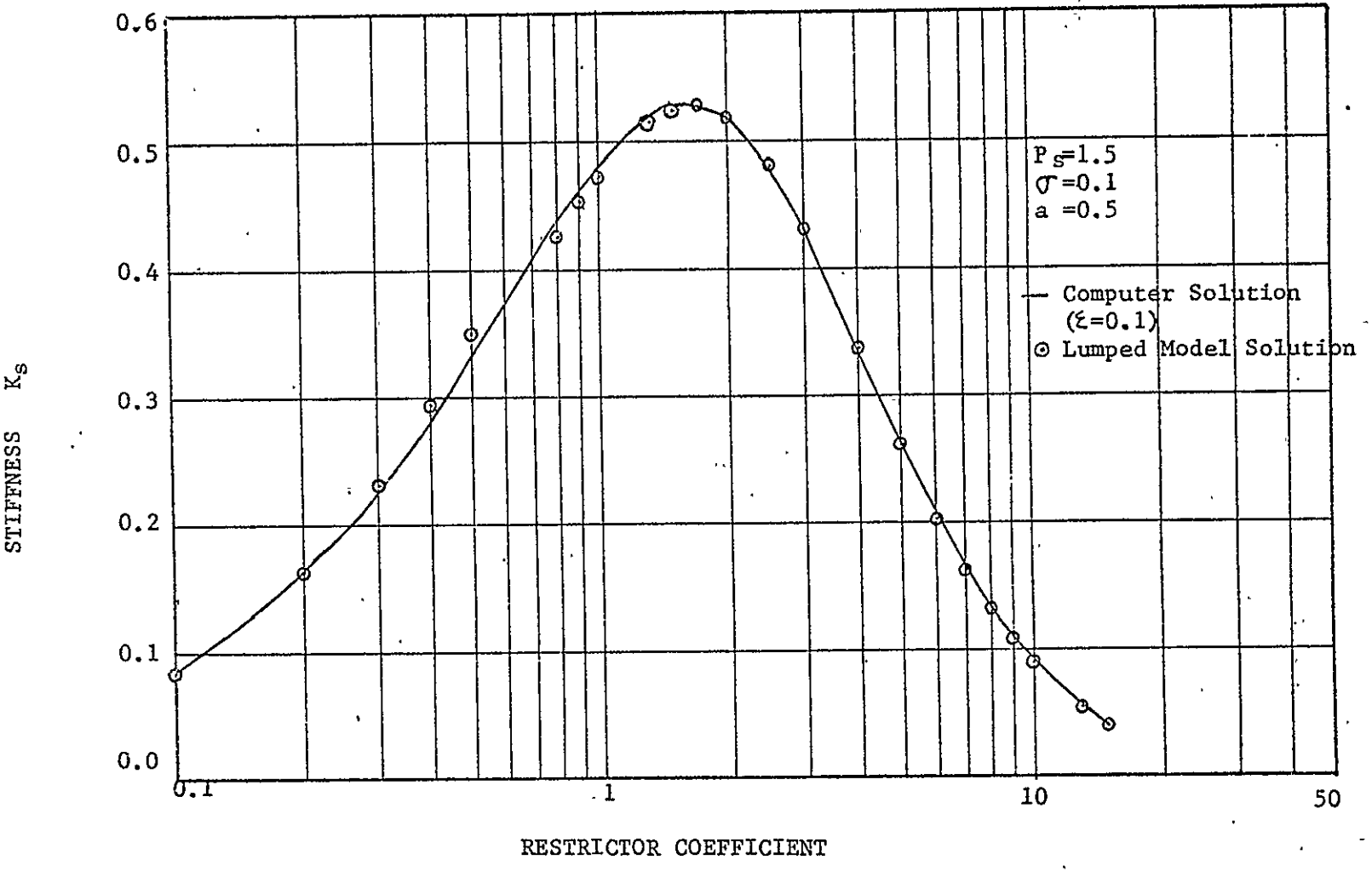

Figure 2. Strip Bearing-Dimensionless Stiffness versus Restrictor Coefficient (P_s=1.5, σ=0.1, a=0.5)

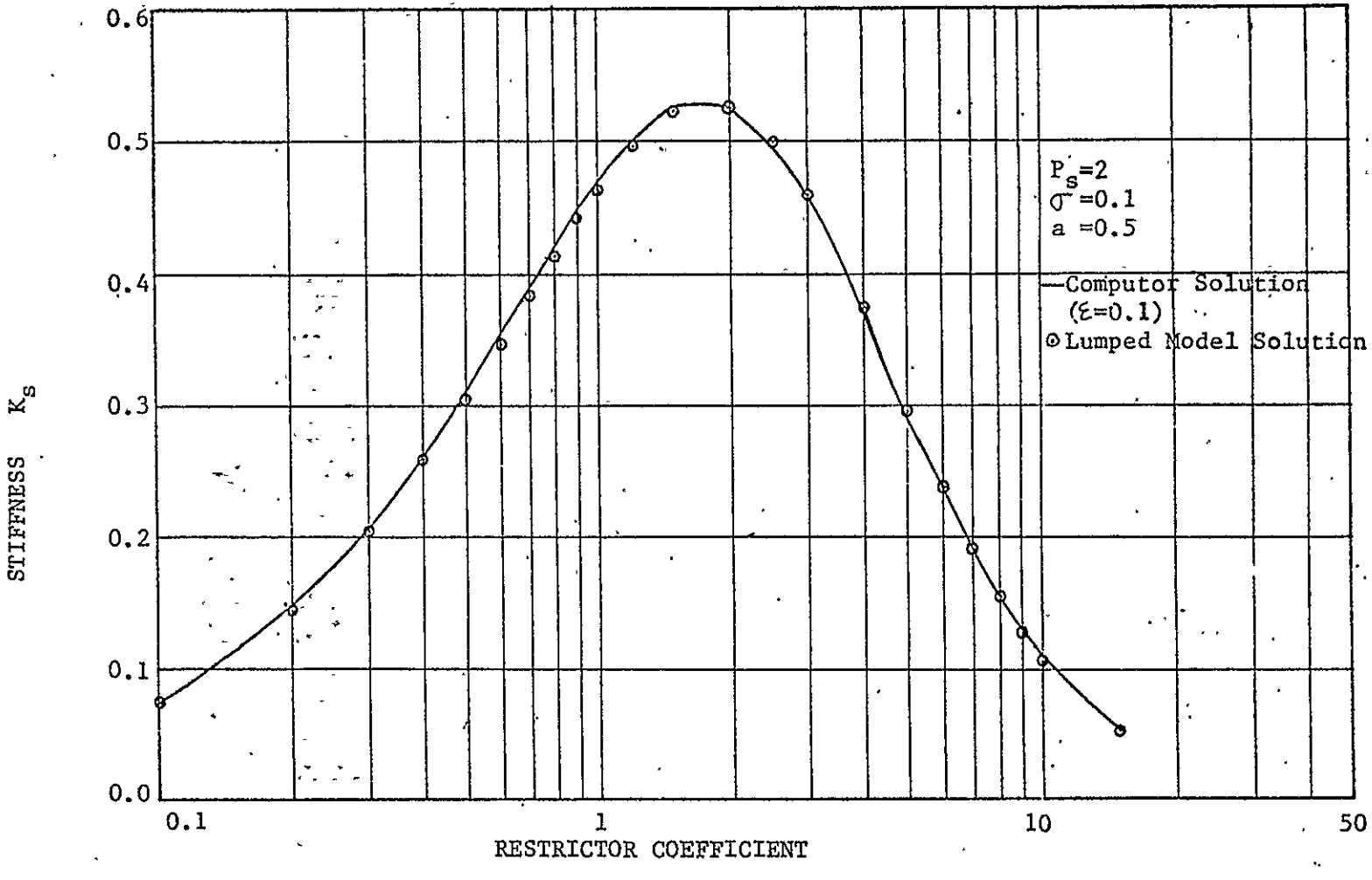

Figure 3. Strip Bearing-Dimensionless Stiffness versus Restrictor Coefficient (P_s=2, σ=0.1, a=0.5)

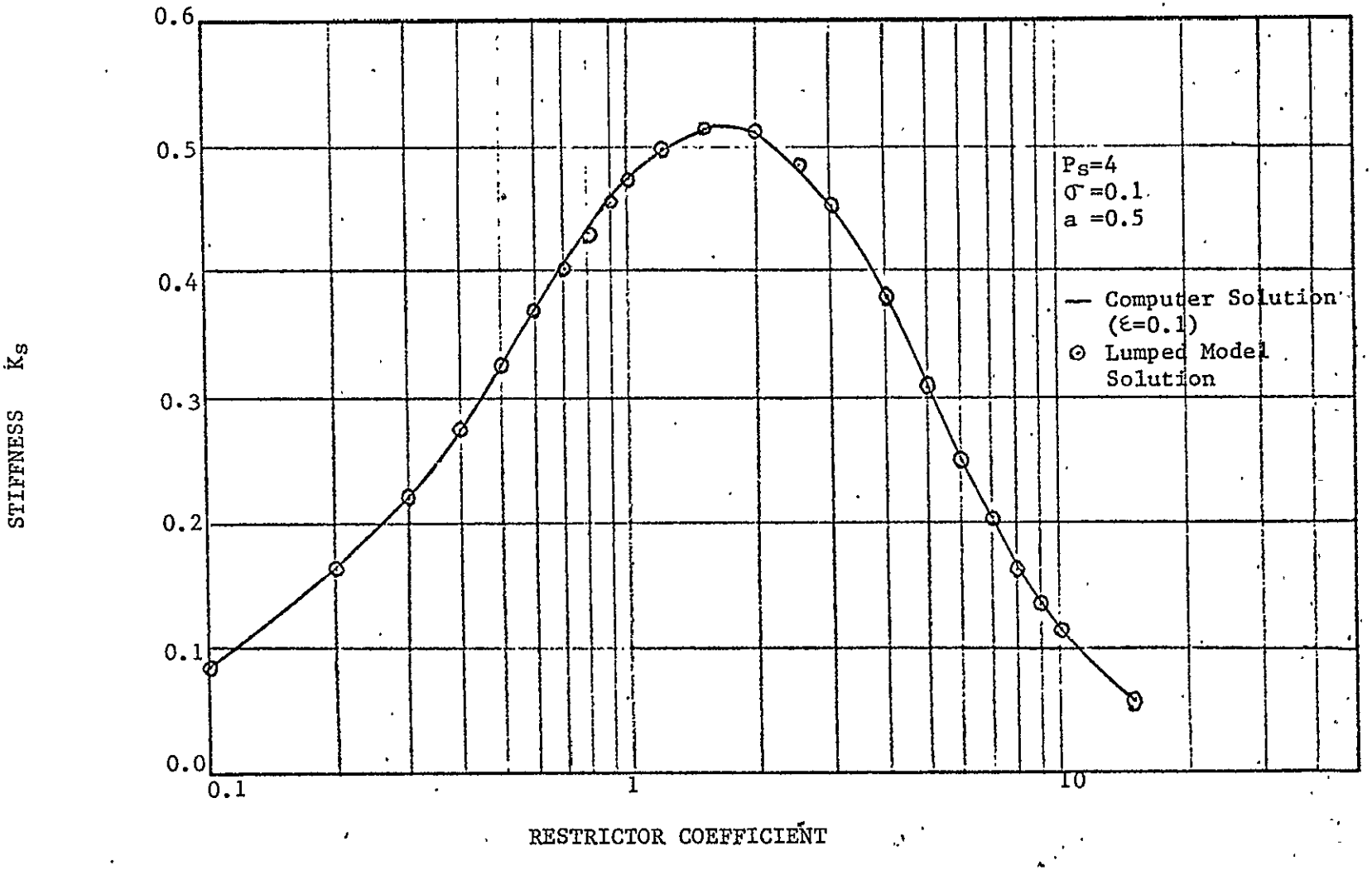

Figure 4. Strip Bearing-Dimensionless Stiffness versus Restrictor Coefficient (P_s=4, σ=0.1, a=0.5)

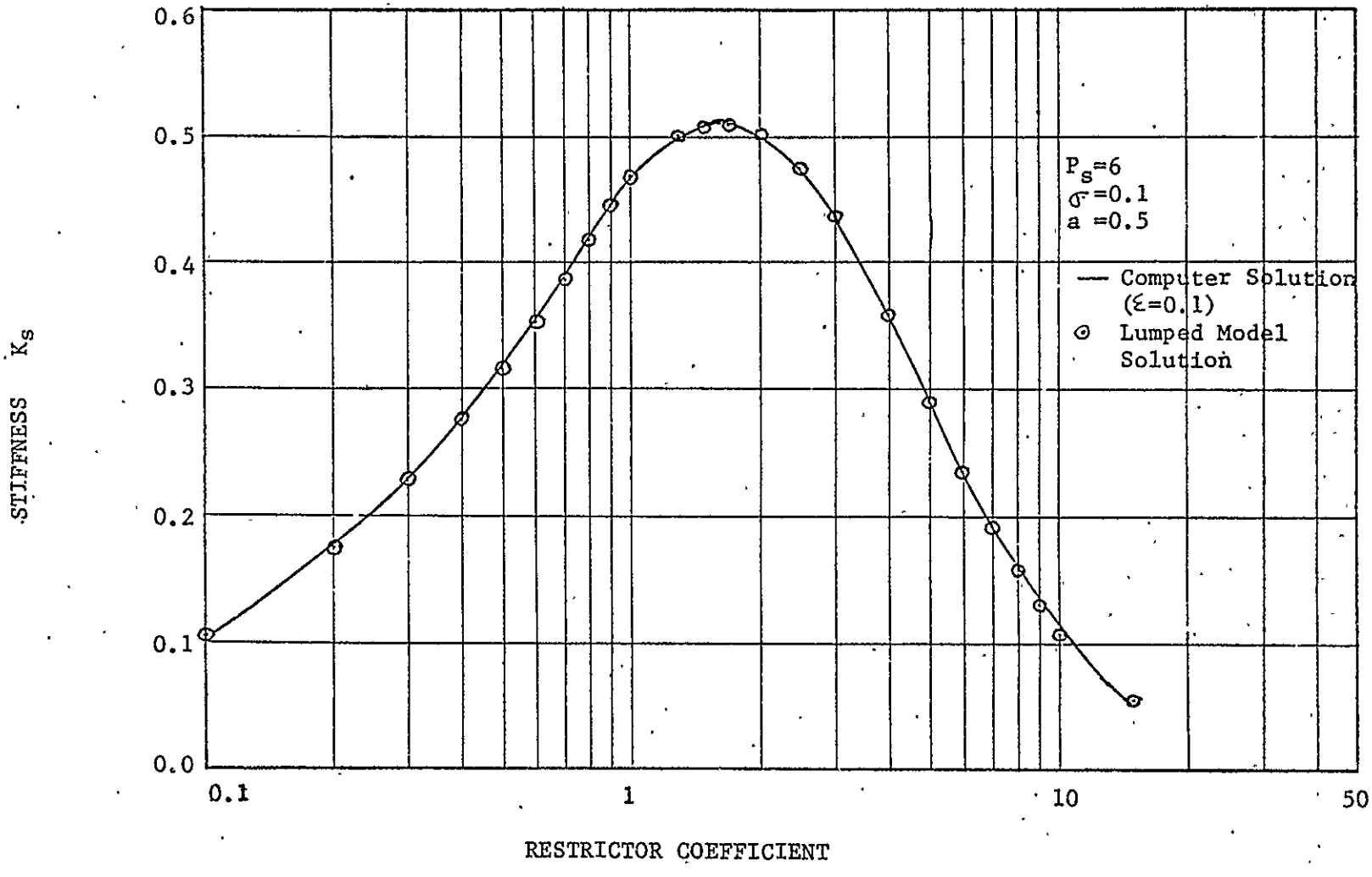

Figure 5. Strip Bearing-Dimensionless Stiffness versus Restrictor Coefficient (P_s=6, σ=0.1, a=0.5)

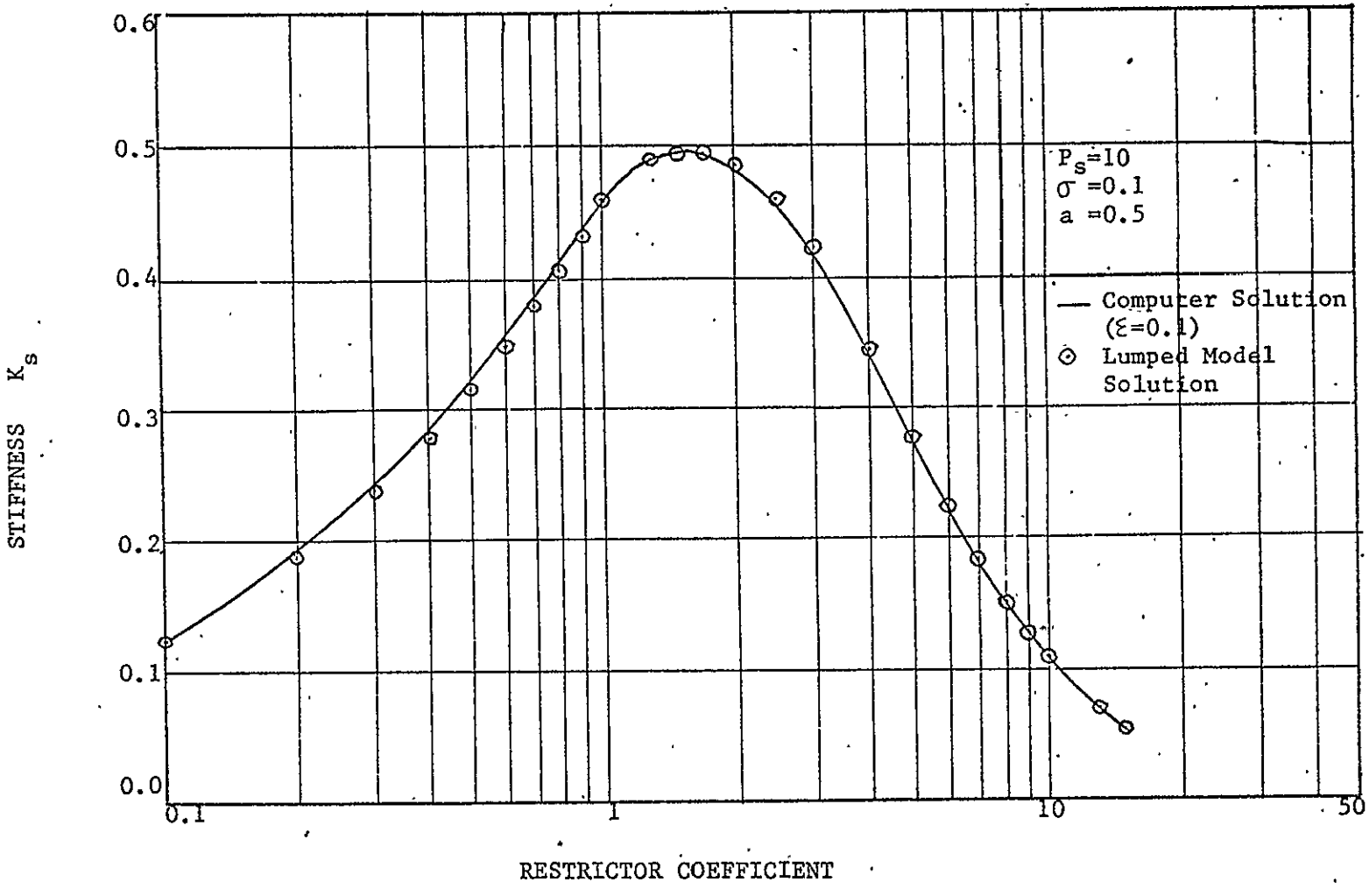

Figure 6. Strip Bearing-Dimensionless Stiffness versus Restrictor coefficient (P_s=10, σ=0.1, a=0.5)

3.2 Damping

The relationship between the dimensionless damping, C, and the restrictor coefficient, Λ, is shown in Figures 7-11. It can be observed that the dimensionless damping is highly dependent on the restrictor coefficient and the supply pressure. As the restrictor coefficient approaches zero, the damping approaches a constant. As the restrictor coefficient approaches infinity, the damping approaches a smaller constant. These values represent the extremes for pure squeeze films [10] i.e. no inlets ($\Lambda=0$) or inlets open to the ambient ($\Lambda=\infty$).

Comparing the damping between computer solutions by Stiffler and Tapia [9] and lumped parameter approach by this study, it is observed that the lumped model agrees well with computer solutions for the range of lower restrictor coefficients, $\Lambda<1.0$, but differences occur in the range of larger restrictor coefficients. These results indicate that a lumped model for the damping is not entirely adequate. Sadd and Stiffler [10] have shown that pure squeeze films ($\Lambda=0,\infty$) display quite different damping depending on the geometry. However, the lumped model would display no difference between a strip and a square, for example, if their corresponding film volumes were identical.

3.3 Squeeze Number

To introduce the squeeze number, σ, into equations (2-37), (2-38), (2-42a), and (2-43a), the dimensionless stiffness and damping can be expressed as follows:

when

$$\frac{P_{ro}}{P_s} > \left(\frac{2}{k+1}\right)^{\frac{k}{k-1}},$$

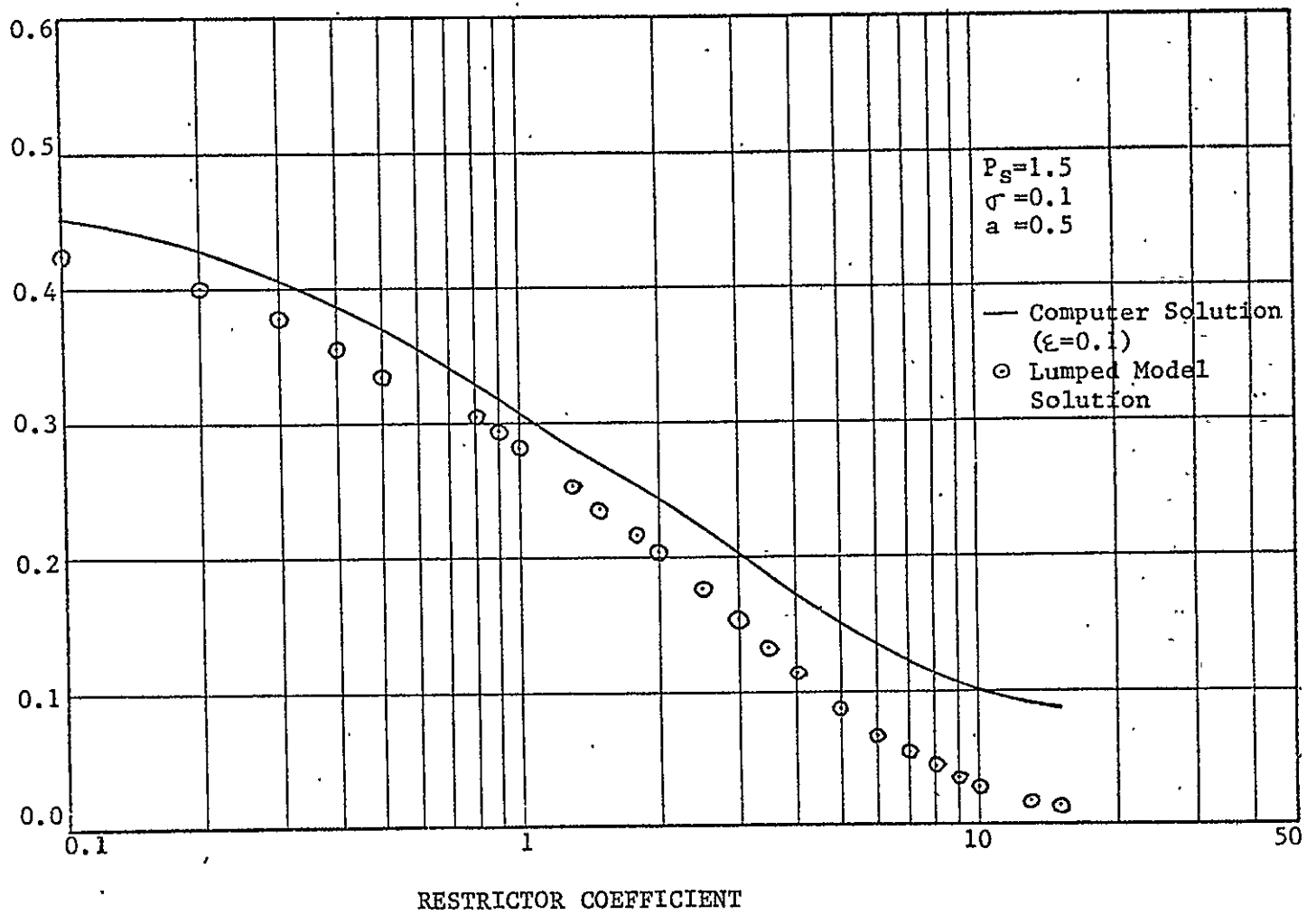

Figure 7. Strip Bearing-Dimensionless Stiffness versus Restrictor Coefficient (P_S=1.5,σ=0.1, a=0.5)

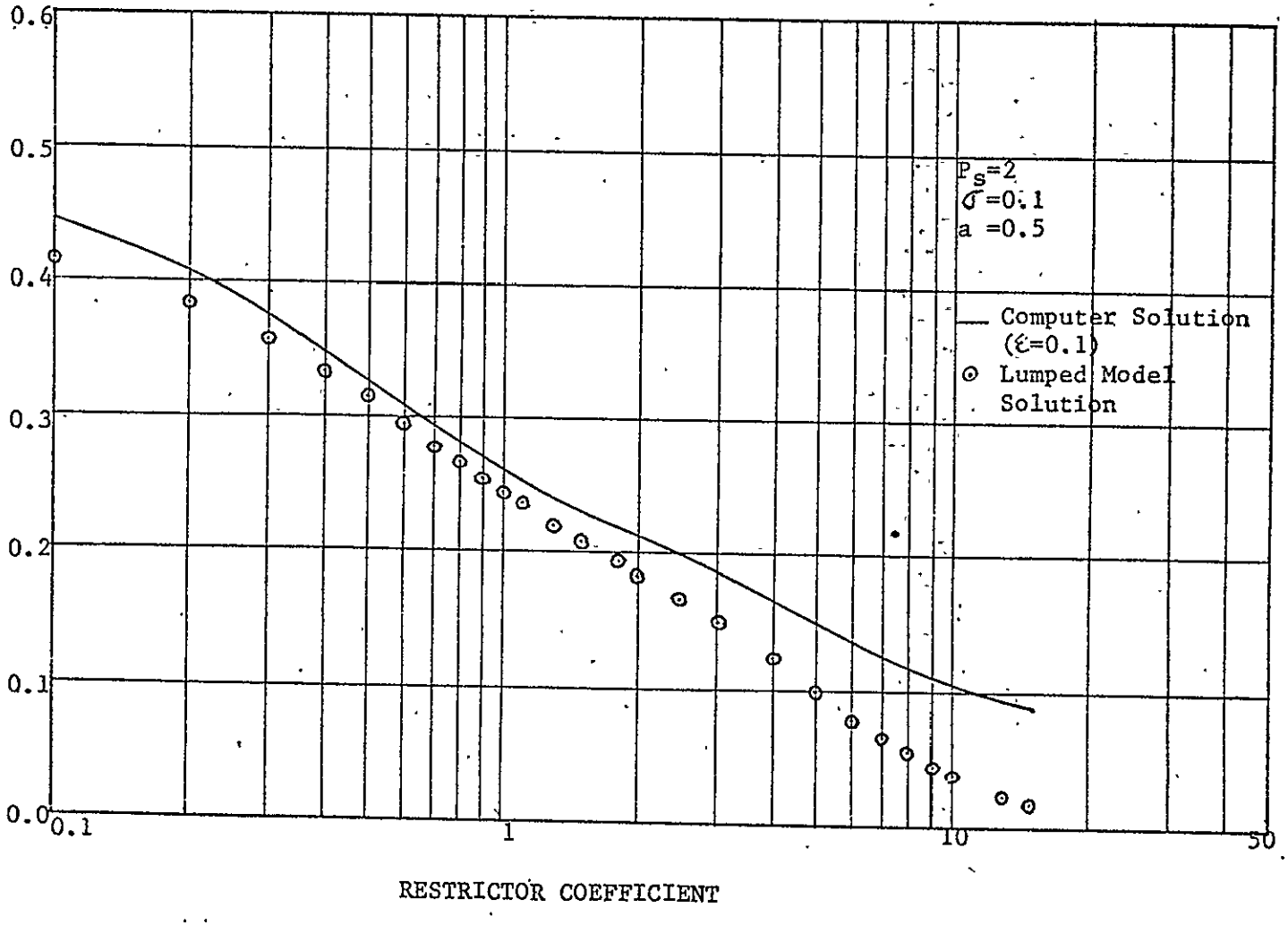

Figure 8. Strip Bearing-Dimensionless Stiffness versus Restrictor Coefficient (P_s=2, σ=0.1, a =0.5)

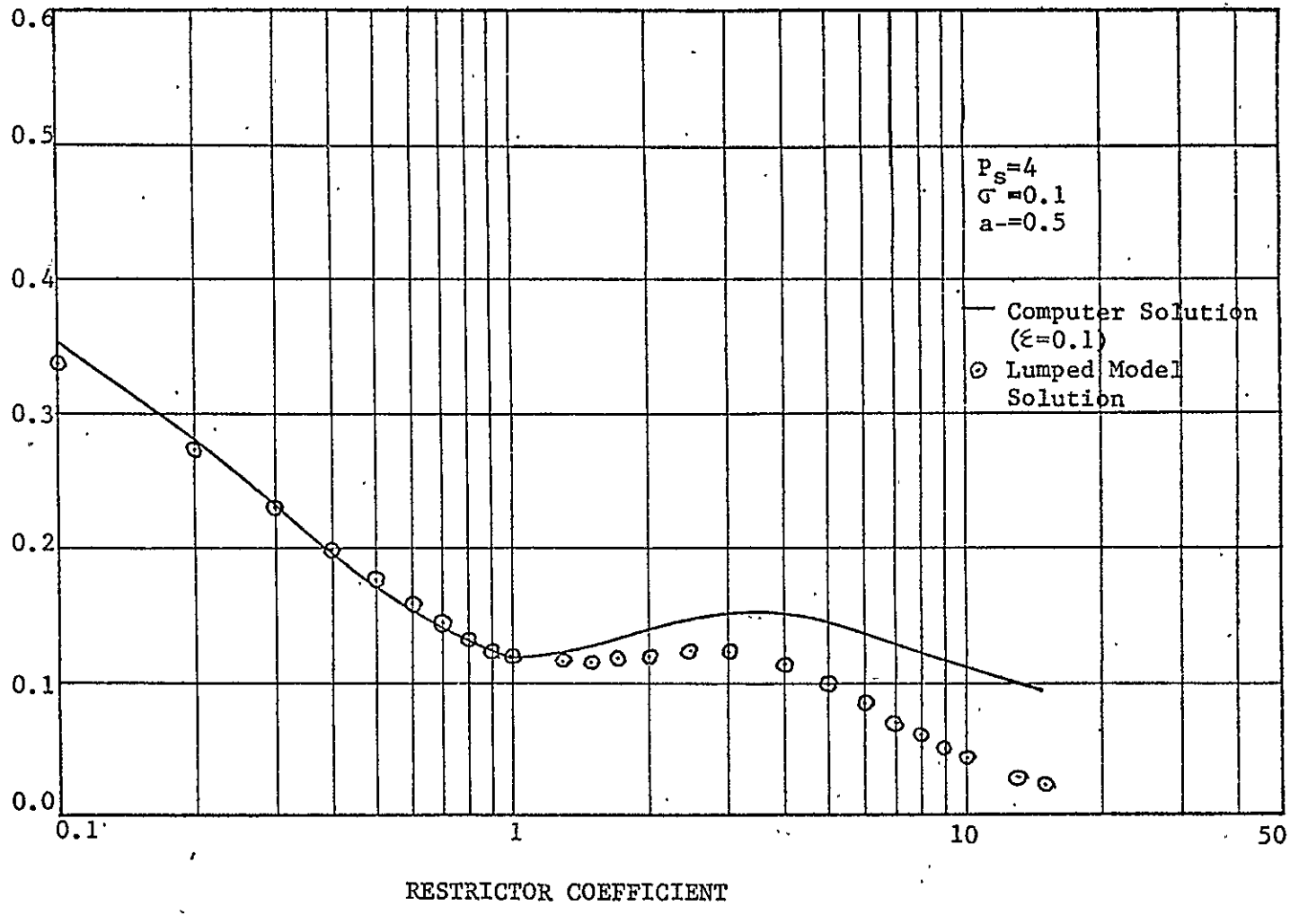

Figure 9. Strip Bearing-Dimensionless Stiffness versus Restrictor Coefficient (P_s=4, σ=0.1, l=0.5)

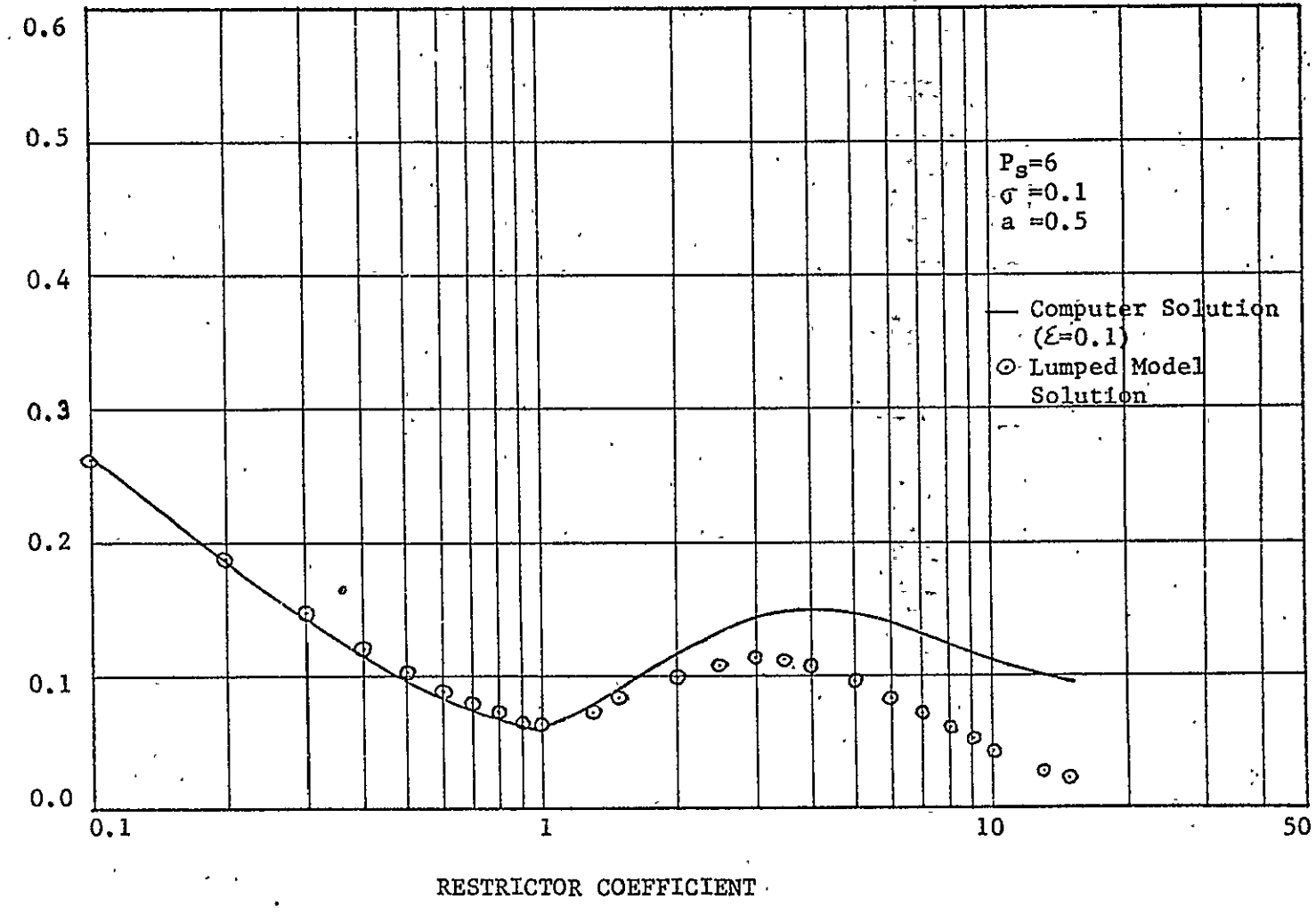

Figure 10. Strip Bearing-Dimensionless Stiffness versus Restrictor Coefficient (P_s=6, σ=0.1, a=0.5)

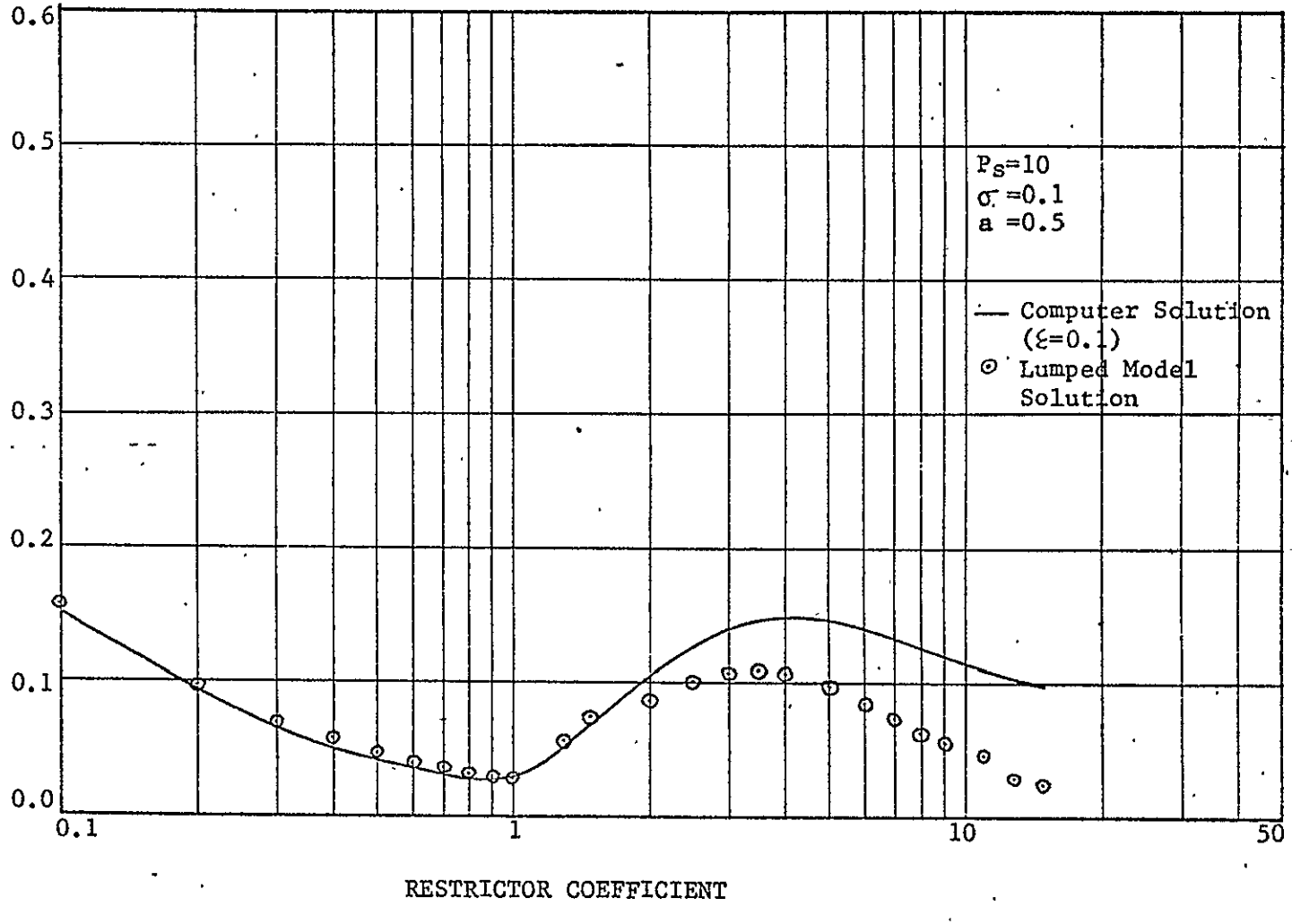

Figure 11. Strip Bearing-Dimensionless Stiffness versus Restrictor Coefficient (P_S=10, σ =0.1, a=0.5)

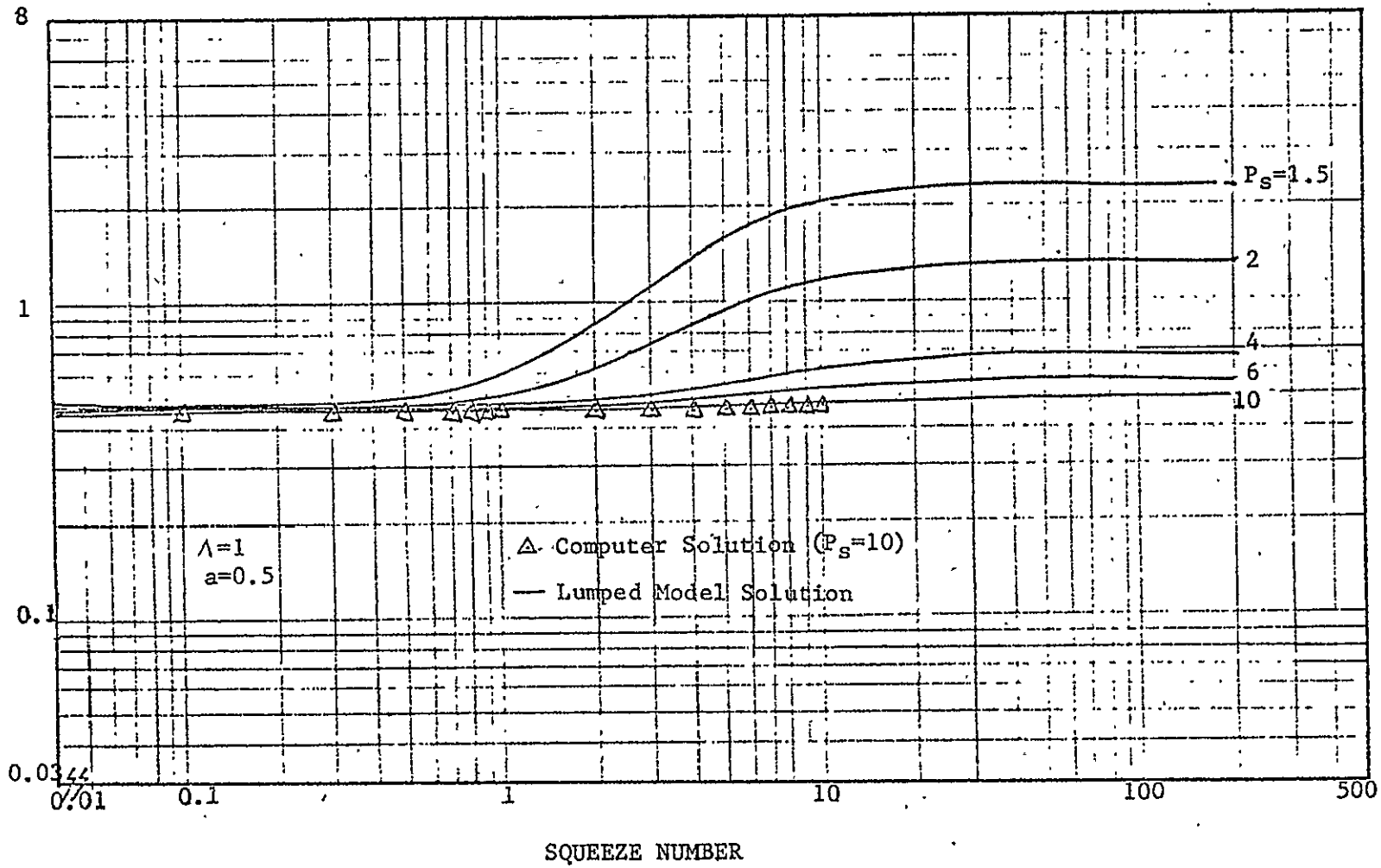

Figure 12. Strip Bearing-Dimensionless Stiffness versus Squeeze Number (Λ=1, a=0.5)

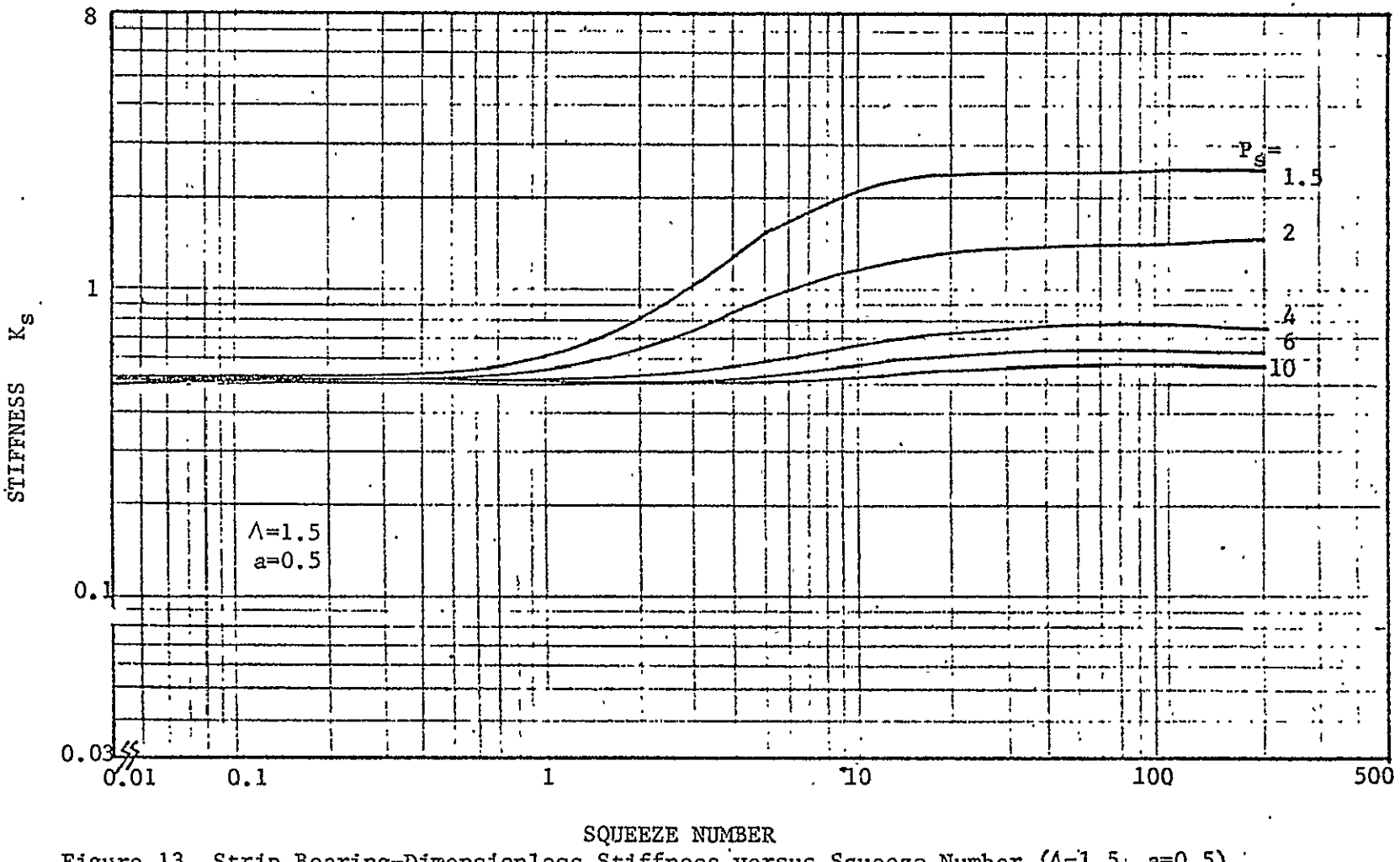

Figure 13. Strip Bearing-Dimensionless Stiffness versus Squeeze Number (Λ=1.5, a=0.5)

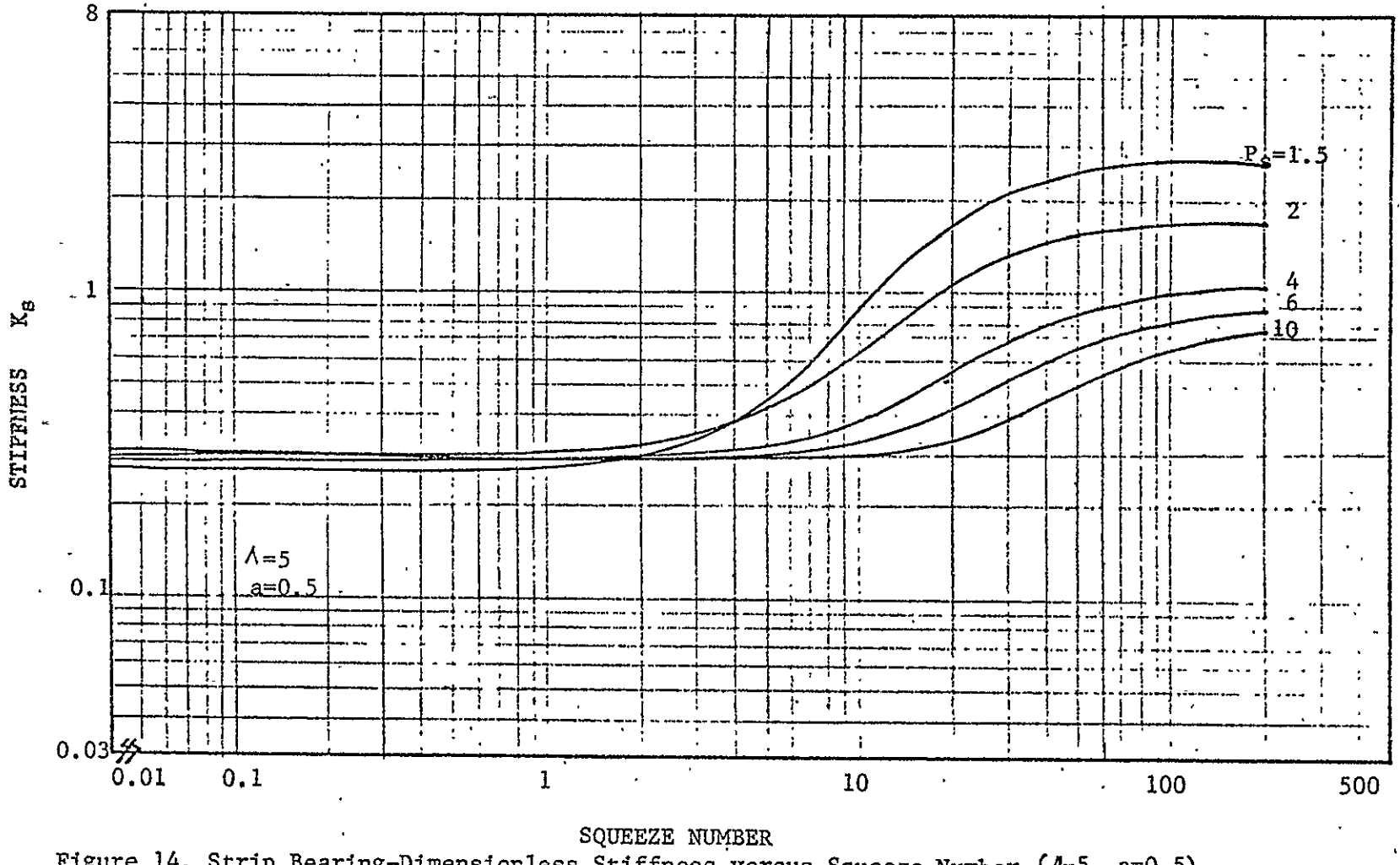

Figure 14. Strip Bearing-Dimensionless Stiffness versus Squeeze Number (Λ=5, a=0.5)

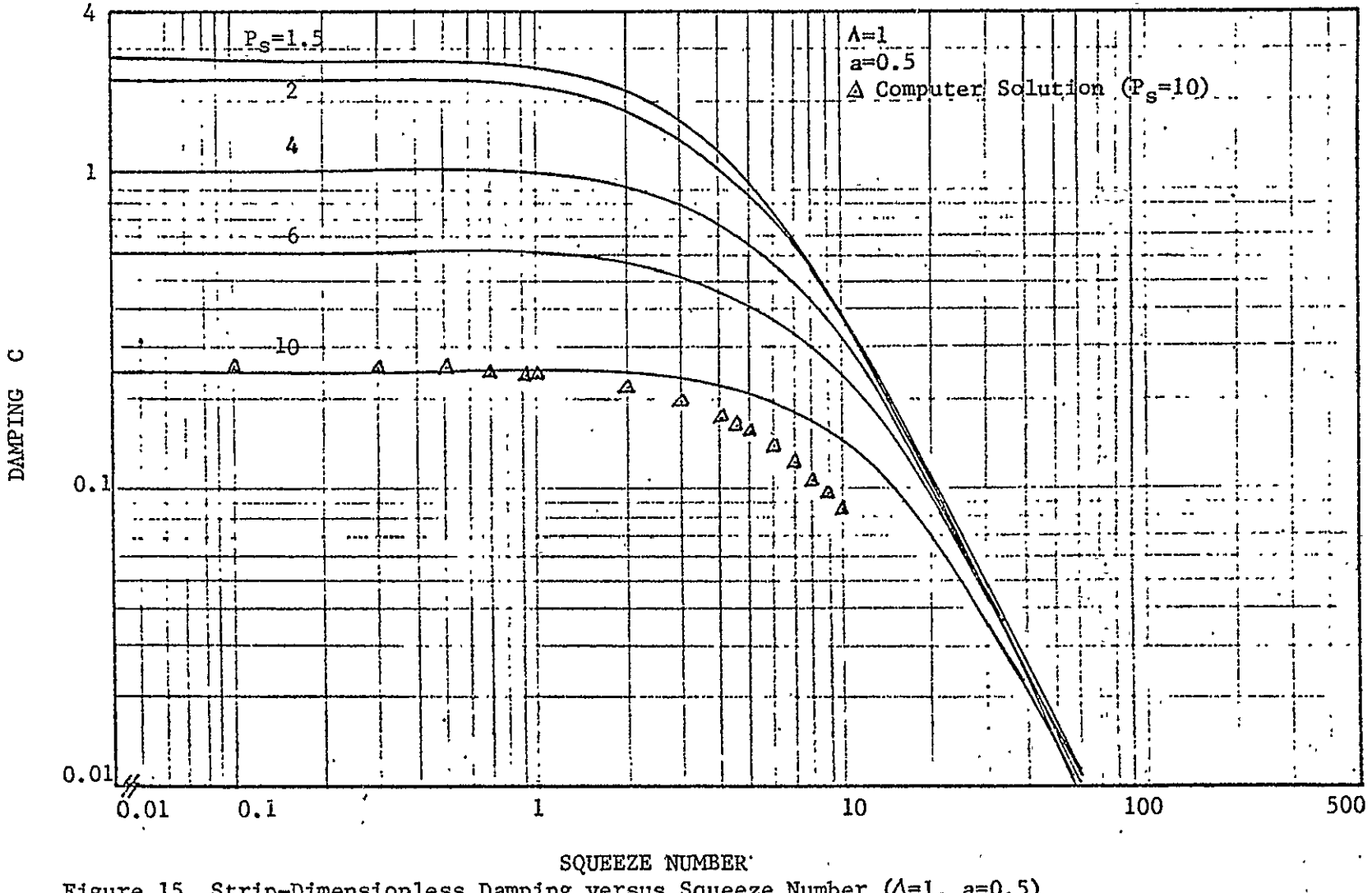

Figure 15. Strip-Dimensionless Damping versus Squeeze Number (Λ=1, a=0.5)

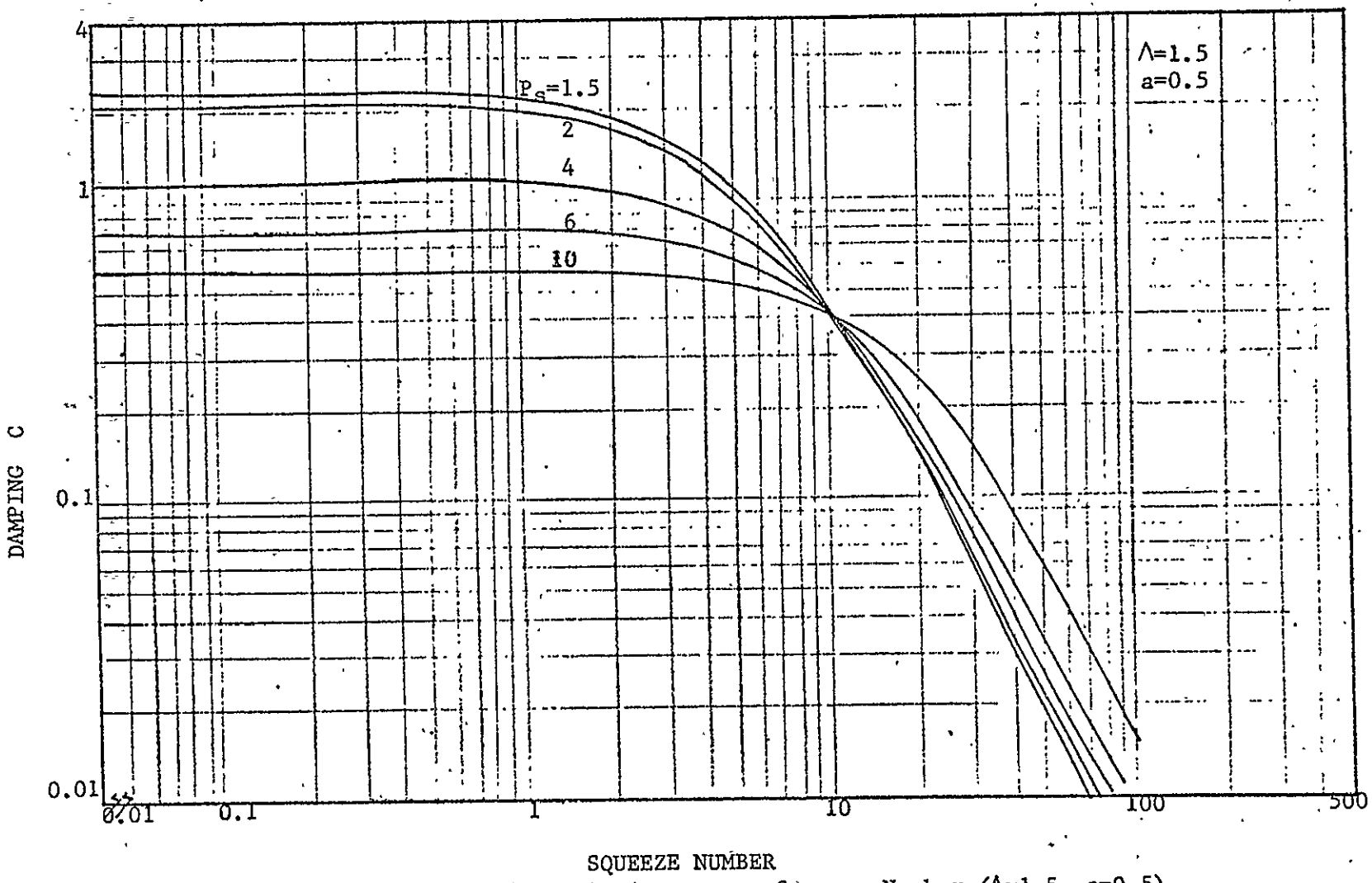

Figure 16. Strip Bearing-Dimensionless Damping versus Squeeze Number (Λ=1.5, a=0.5)

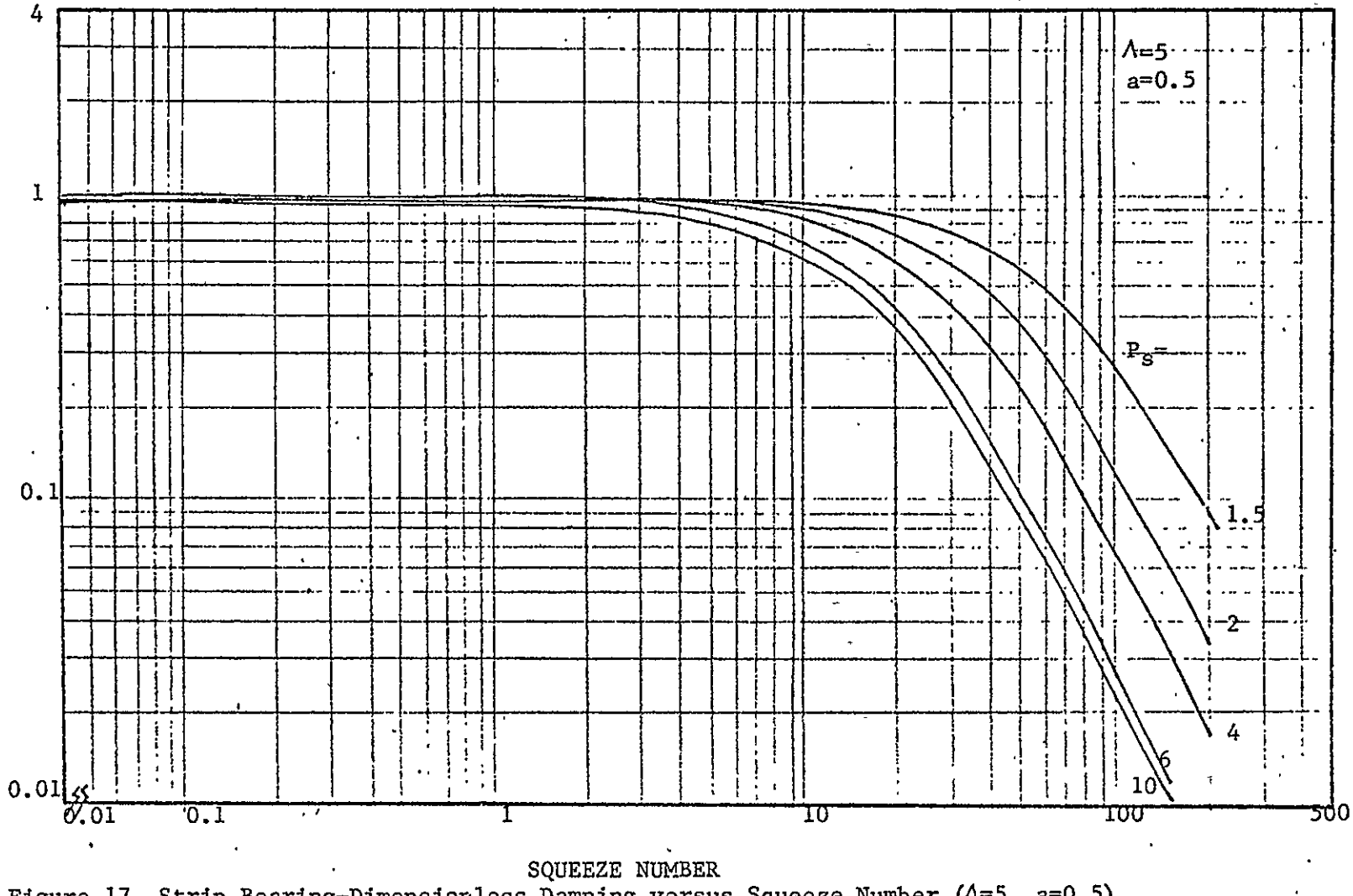

Figure 17. Strip Bearing-Dimensionless Damping versus Squeeze Number (Λ=5, a=0.5)

$$K_s = k_s \left\{ \frac{1 + \frac{1}{144} k_s (P_s - 1) \left(\frac{\sigma}{m_o}\right)^2 \left[\lambda P_{ro} + \frac{2}{3}(1-\lambda) \left(\frac{P_{ro}^3 - 1}{P_{ro}^2 - 1} \right) \right]}{1 + \frac{1}{144} \left[k_s (P_s - 1) \frac{\sigma}{m_o} \right]^2} \right\} \qquad (3\text{-}1)$$

$$C = \frac{k_s (P_s - 1)/m_o \left\{ \lambda P_{ro} + \frac{2}{3}(1-\lambda) \left(\frac{P_{ro}^3 - 1}{P_{ro}^2 - 1} \right) - k_s (P_s - 1) \right\}}{1 + \frac{1}{144} \left[k_s (P_s - 1) \frac{\sigma}{m_o} \right]^2}$$

where

$$k_s = \left(\frac{P_{ro}^2 - 1}{P_s - 1} \right) \left\{ \frac{\lambda + \frac{2}{3}(1-\lambda) \left(\frac{P_{ro}}{P_{ro}^2 - 1} \right) \left[3P_{ro} - 2 \left(\frac{P_{ro}^3 - 1}{P_{ro}^2 - 1} \right) \right]}{P_{ro} - \left(\frac{P_{ro}^2 - 1}{2kP_{ro}} \right) \left\{ 1 - \left(\frac{P_{ro}}{P_s} \right)^{\frac{k-1}{k}} \frac{(k-1)}{2 \left[1 - \left(\frac{P_{ro}}{P_s} \right)^{\frac{k-1}{k}} \right]} \right\}} \right\} \qquad (3\text{-}3)$$

or when

$$\frac{P_{ro}}{P_s} \leq \left(\frac{2}{k+1} \right)^{\frac{k}{k-1}},$$

$$K_s = k_s \frac{1 + \frac{1}{144} k_s (P_s - 1) \left(\frac{\sigma}{m_o} \right)^2 \left[aP_{ro} + \frac{2}{3}(1-a) \left(\frac{P_{ro}^3 - 1}{P_{ro}^2 - 1} \right) \right]}{1 + \frac{1}{144} \left[k_s (P_s - 1) \frac{\sigma}{m_o} \right]^2} \qquad (3\text{-}4)$$

$$C = \frac{k_s(P_s - 1)/m_o \left\{ \lambda P_{ro} + \frac{2}{3}(1-\lambda) \left(\frac{P_{ro}^3 - 1}{P_{ro}^2 - 1} \right) - k_s(P_s - 1) \right\}}{1 + \frac{1}{144} \left[k_s(P_s - 1) \frac{\sigma}{m_o} \right]^2} \qquad (3\text{-}5)$$

where

$$k_s = \left(\frac{P_{ro}^2 - 1}{P_s - 1} \right) \left\{ \frac{\lambda + \frac{2}{3}(1-\lambda) \left(\frac{P_{ro}}{P_{ro}^2 - 1} \right) \left[3P_{ro} - 2 \left(\frac{P_{ro}^3 - 1}{P_{ro}^2 - 1} \right) \right]}{P_{ro}} \right\} \qquad (3\text{-}6)$$

The effect of squeeze numbers on the stiffness and damping is shown in Figures 12-17. It is found that low squeeze number ($\sigma < 1$) has little effect on the stiffness and damping. However, the stiffness increases and the damping decreases for large squeeze numbers.

Computer solutions are available for $P_s=10, \Lambda=1$ and are presented in Figures 12,13 also. The break frequency for the lumped parameter damping in Figure 15 appears to be realistic in spite of the shortcomings reported in Section 3.2.

CHAPTER IV

ANALYSIS OF THE SQUARE BEARING

4.1 The Square Bearing (Condensed from REFERENCE [8])

To analyze the square bearing, it is also divided into two regions (Figure 18) as the previous strip bearing. From the symmetry of the geometry, one-quarter of the square bearing is considered here, and an inherently equivalent line source is used to replace the discrete inlets.

The Reynolds' equation, equation (2-1), can be normalized using previous dimensionless variables by using the length L* in place of width w^*.

Thus,

$$\frac{\partial^2}{\partial x^2}(P^2) + \frac{\partial^2}{\partial z^2}(P^2) = \frac{2\sigma}{h^3}\frac{\partial}{\partial t}(Ph) \tag{4-1}$$

where the squeeze number, σ, is defined as

$$\sigma = \frac{12\mu\Omega^* L^{*2}}{h_o^{*2} P_a^*} \tag{4-2}$$

The average mass flow across the sill area is given by REFERENCE [8] as

$$m_o^* = \frac{P_a^* h_o^{*3}}{2\mu RT} m_o \tag{4-3}$$

where

$$m_o = \frac{(P_{ro}^2 - 1) F}{3} \tag{4-4}$$

and F is given for the three different span ratio in the following table:

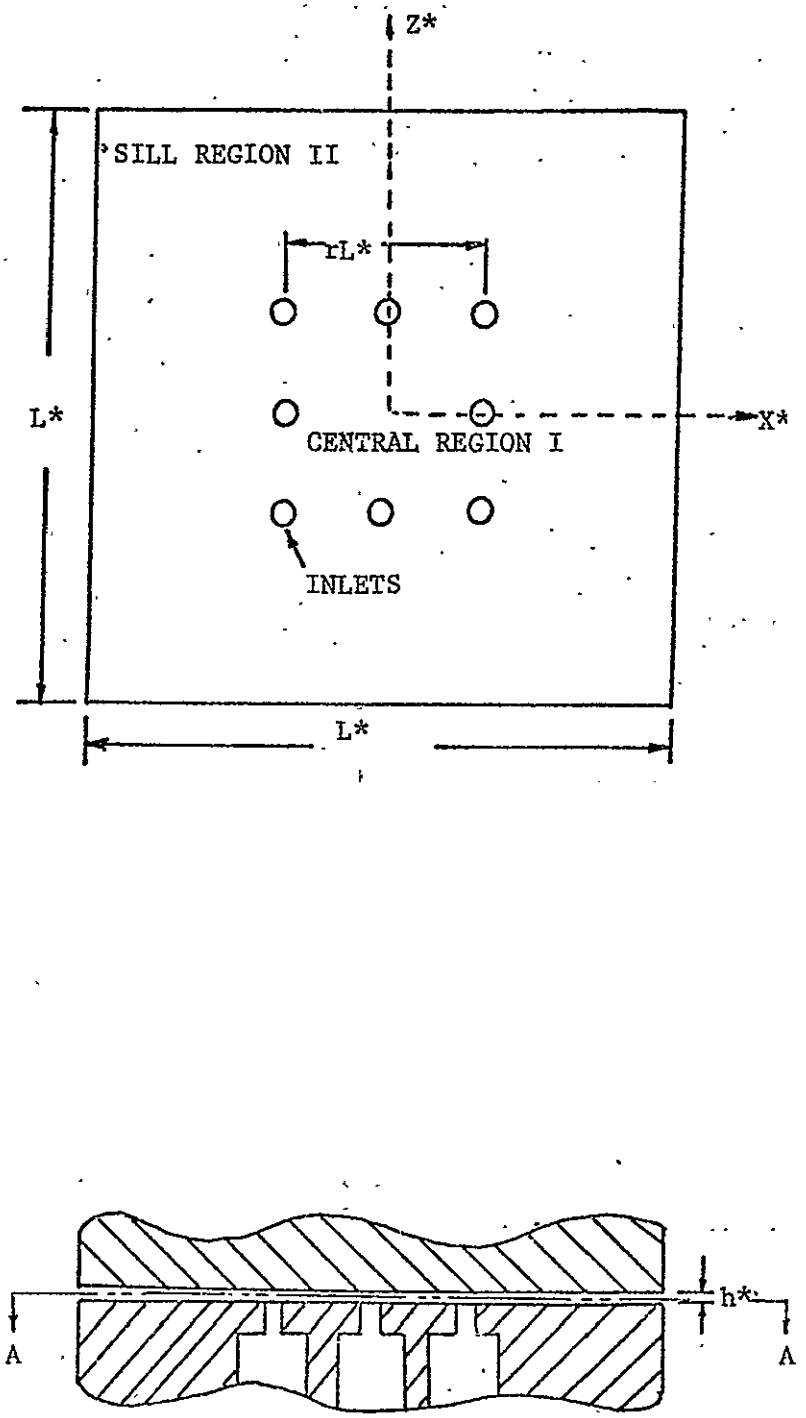

Figure 18. Inherently Compensated, Square, Thrust Bearing

r	F
0.4	1.83
0.6	3.48
0.8	8.44

From the flow continuity, equation (2-7), for the average mass flow across the bearing, the average pressure downstream of the orifice, P_{ro}, is determined by equations (2-14) and (2-15) except that now the coefficient, Λ, is

$$\Lambda = \frac{6 C_D N \pi d_o^* \mu}{P_s P_a^* h_o^{*2} F} \left(\frac{2 g_o k R T}{k - 1} \right)^{\frac{1}{2}} \tag{4-5}$$

The bearing load capacity is given by

$$W^* = 4 \int_o^{L^*/2} \int_o^{L^*/2} (P^* - P_a^*) \, dx^* \, dz^*$$

$$= 4 L^{*2} P_a^* \int_o^{\frac{1}{2}} \int_o^{\frac{1}{2}} (P - 1) \, dx \, dz \tag{4-6}$$

Thus, the dimensionless load capacity is

$$W = \frac{W^*}{L^{*2} P_a^*} = 4 \int_o^{\frac{1}{2}} \int_o^{\frac{1}{2}} (P - 1) \, dx \, dz \tag{4-7}$$

In order to apply the lumped parameter model to the square bearing, it is assumed that the average pressure on the sill region is closely approximated by the average sill pressure exhibited by the strip. Then the average load capacity is expressed by

$$W = \lambda (P_r - 1) + (1 - \lambda) \left[\frac{2}{3} \left(\frac{P_r^3 - 1}{P_r^2 - 1} \right) - 1 \right] \qquad (4\text{-}8)$$

where the area ratio, λ, is given in terms of the span ratio, Figure 18, as

$$\lambda = r^2 \qquad (4\text{-}9)$$

The previously developed equations for the strip can be used for the square bearing providing one interprets the results in terms of equation (4-4), (4-5) and (4-9).

CHAPTER V

RESULTS AND MODEL COMPARISONS FOR THE SQUARE BEARING

The stiffness and damping are obtained in this study as functions of restrictor coefficient and supply pressure with inlet location (r = 0.6) fixed. They are compared with computer solutions by Stiffler and Smith [8] at small squeeze number ($\sigma = 0.1$) since the stiffness and damping are insensitive to small squeeze numbers. Design curves for the stiffness and dampling are discussed and compared below for the lumped parameter approach and the computer solutions.

5.1 Stiffness

If the stiffness is compared with computer solutions by Stiffler and Smith [8] as shown in Figures 19,20, it can be observed that the results of the lumped model agree well with computer solutions. However, the stiffness for P_s=2 is greater than it for P_s=6 in the range $1.5 < \Lambda < 5.5$. This fact indicates that the lumped parameter model can not exactly describe the performance of the square bearing, but the agreement is sufficient for most engineering purposes.

5.2 Damping

Comparing the damping between computer solutions by Stiffler and Smith [8] and the lumped parameter approach by this study, the results show that the lumped parameter model is not adequate enough to describe the performance of the square bearing. Sadd and Stiffler [10] have shown that the damping for the squeeze bearing is approximately one-half of the damping for the strip bearing in the case of

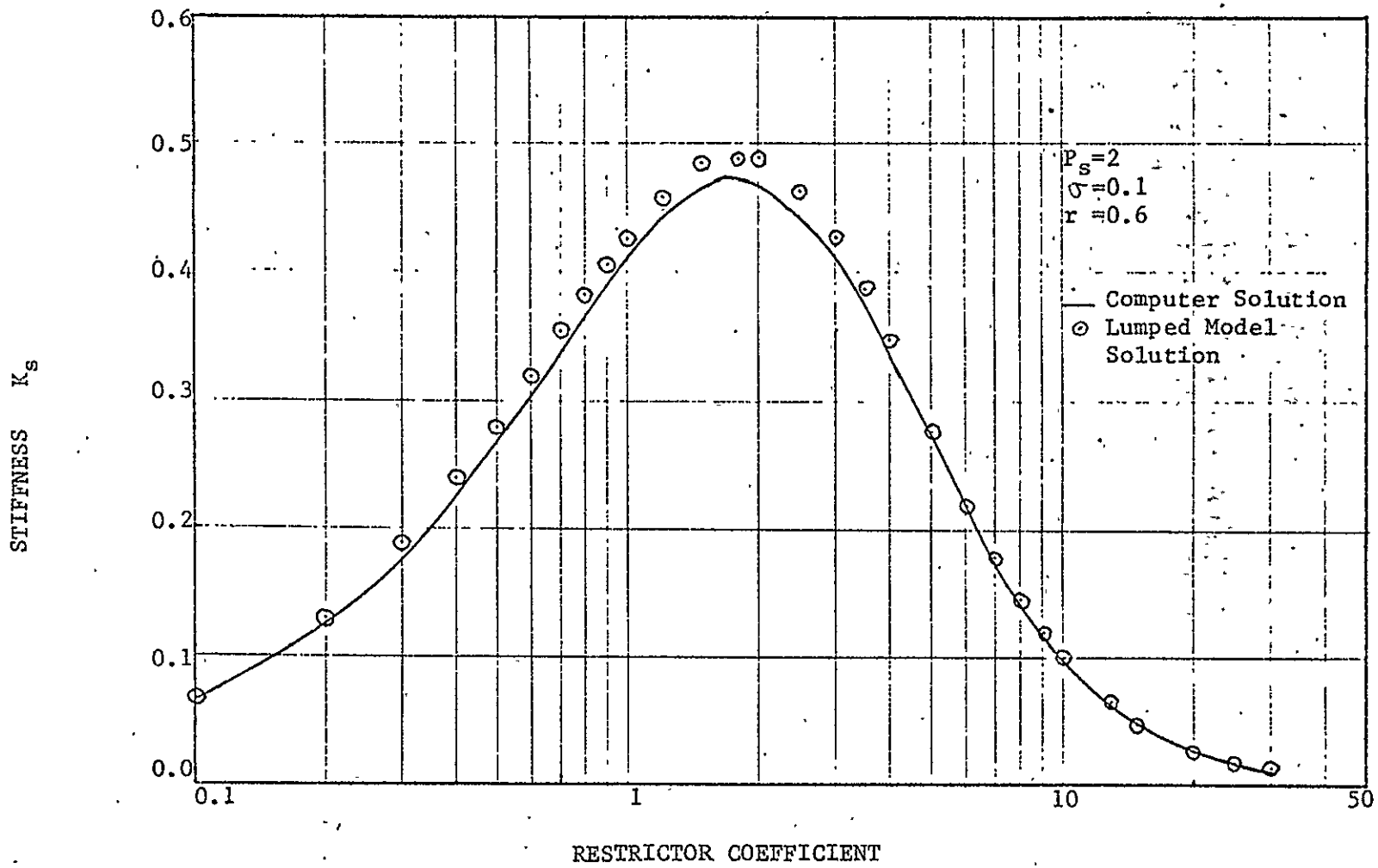

Figure 19. Square Bearing-Dimensionless Stiffness versus Restrictor Coefficient (P_s=2, σ=0.1, r=0.6)

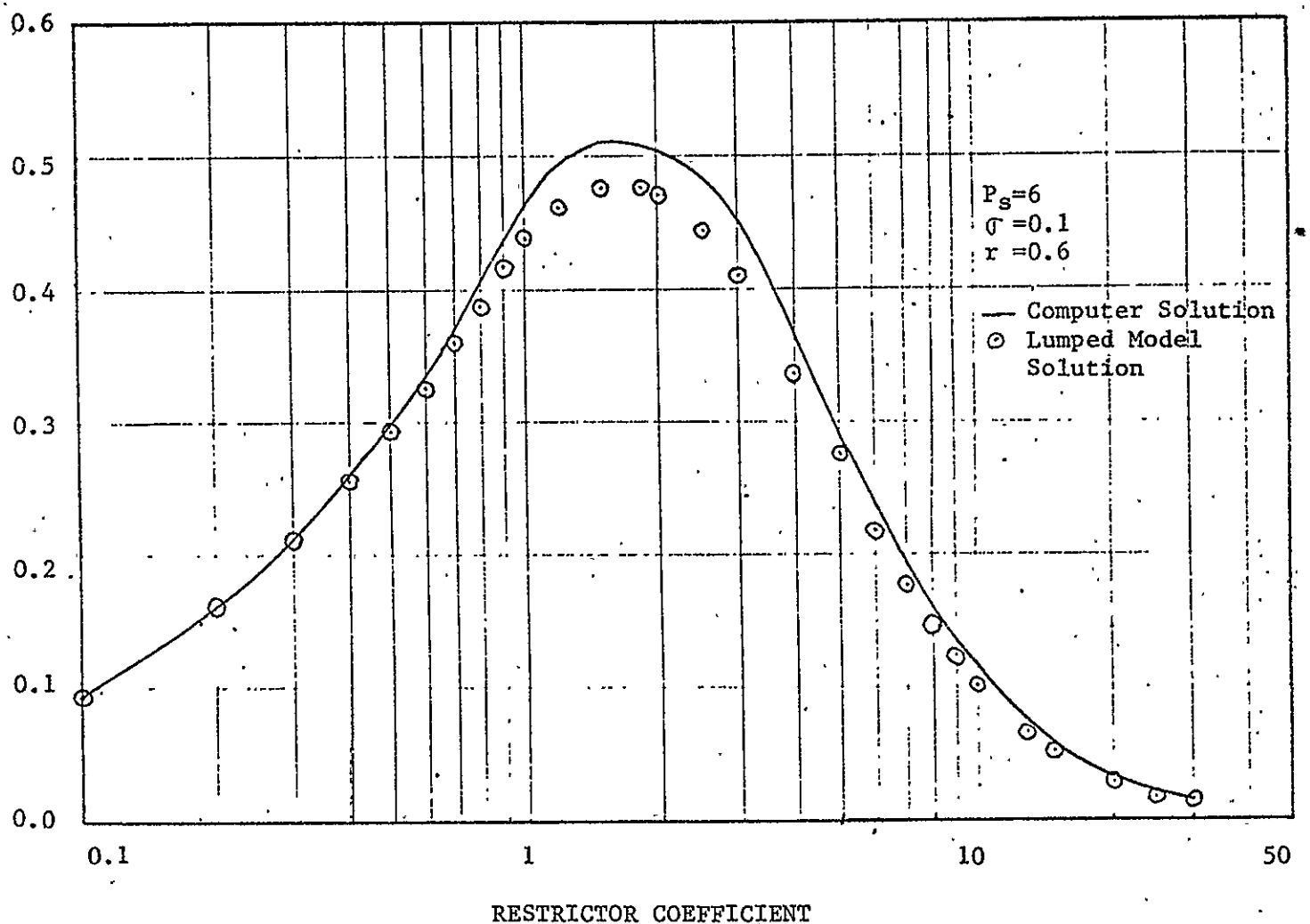

Figure 20. Square Bearing-Dimensionless Stiffness versus Restrictor Coefficient (P_s=6, σ=0.1, r=0.6)

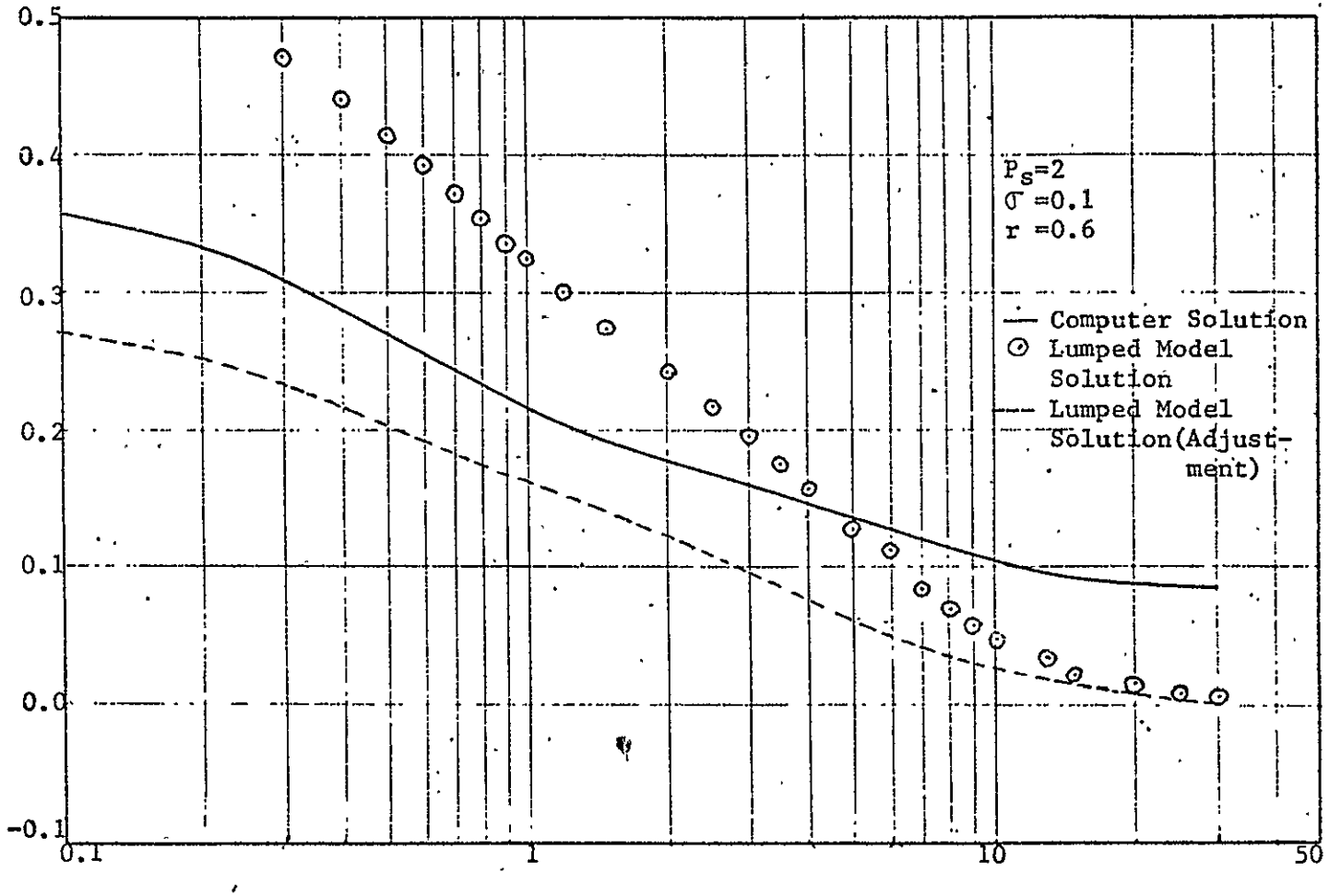

Figure 21. Square Bearing-Dimensionless Damping versus Restrictor Coefficient (P_s=2, σ=0.1, r=0.6)

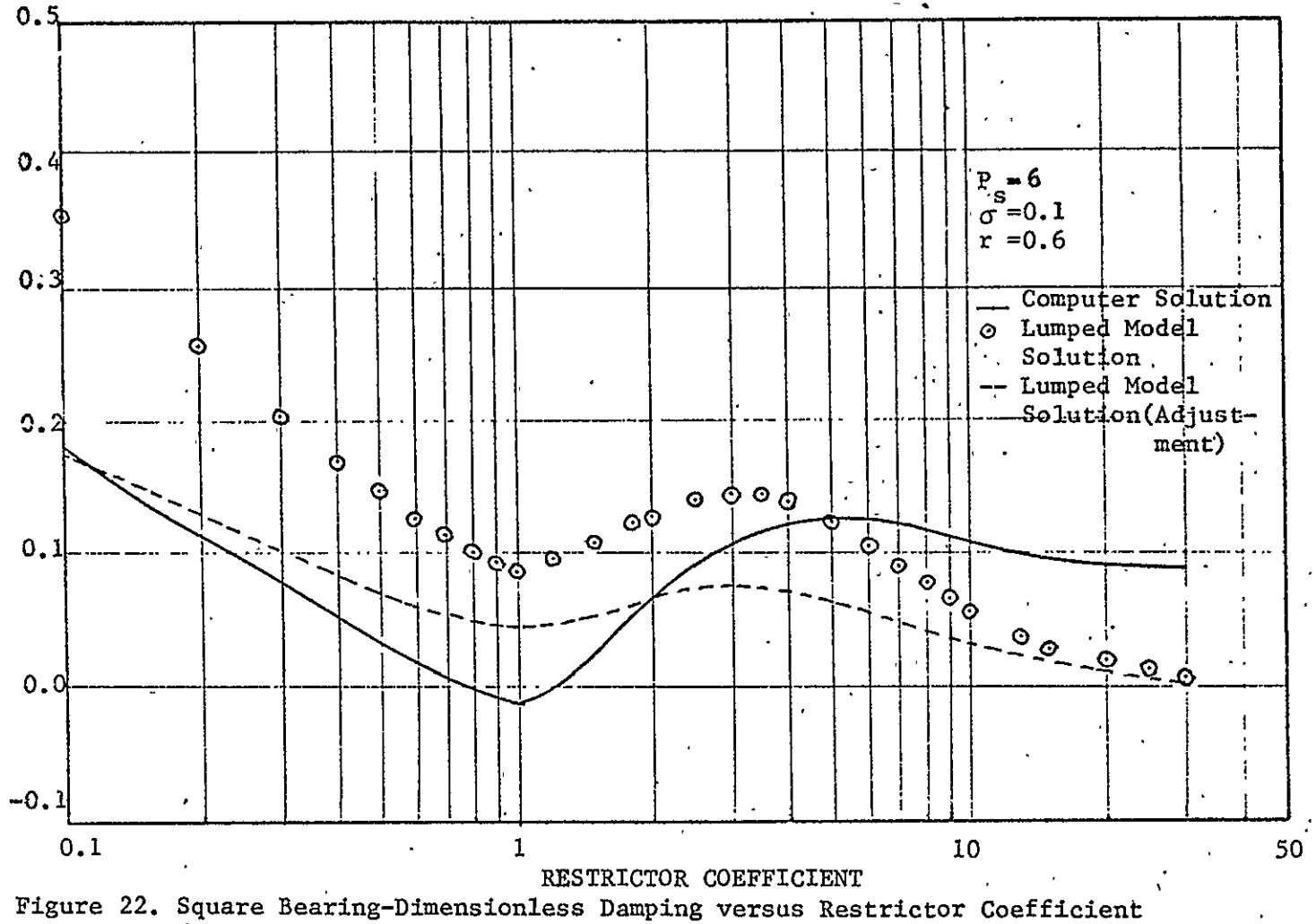

Figure 22. Square Bearing-Dimensionless Damping versus Restrictor Coefficient (P_s=6, σ=0.1, r=0.6)

pure squeeze film ($\Lambda=0$). So if the damping from the lumped parameter approach is adjusted by the factor 1/2, the results are improved but the agreement could not be described as sufficiently accurate.

5.3 Squeeze Number

Comparing with computer solutions[8] in Figures 23-26, it is observed that the break frequencies for the lumped parameter model appear to agree well with the computer model in spite of the inadequacy of the model as indicated in Section 3.2. According to this result and observing equation (2-38), the term ζ_2, which indicates the compressibility effect of the bearing film alone controls the break frequency. Thus, the term ζ_1 which indicates the volume effect of bearing film would appear to be the target variable in attemps to improve the lumped model for damping.

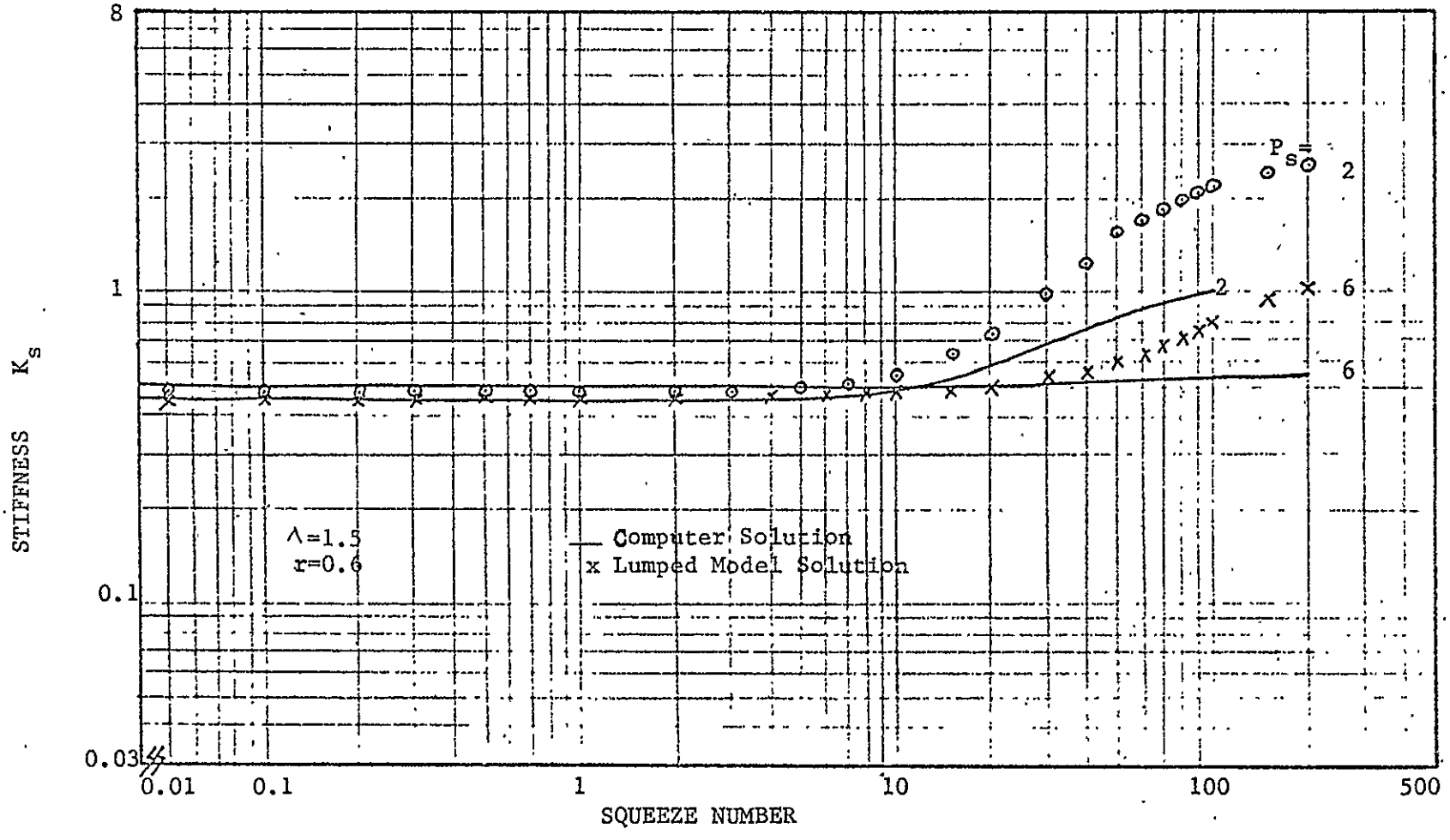

Figure 23. Square Bearing-Dimensionless Stiffness versus Sqeeze Number (Λ=1.5, r=0.6)

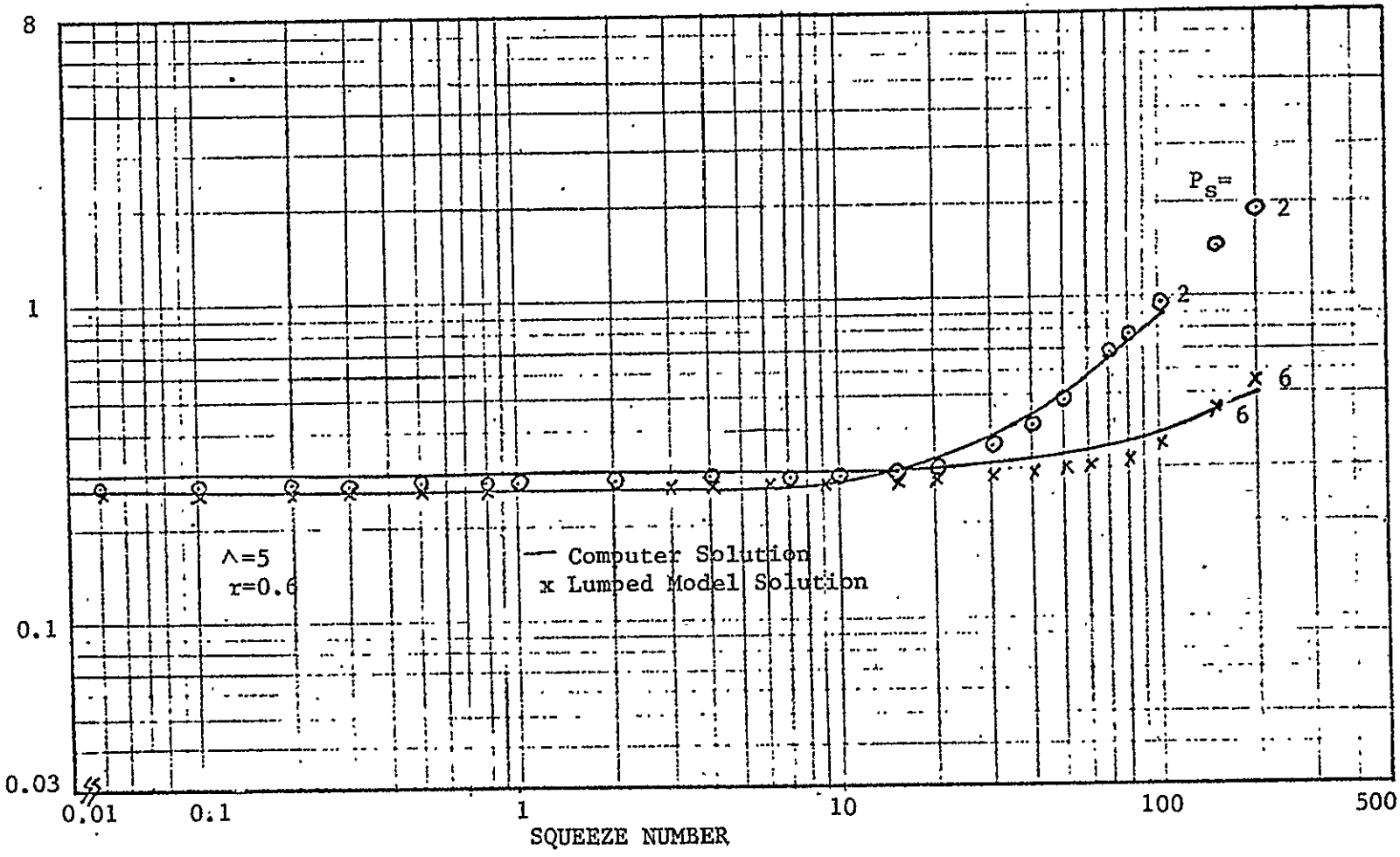

Figure 24. Square Bearing-Dimensionless Stiffness versus Squeeze Number (Λ =5, r=0.6)

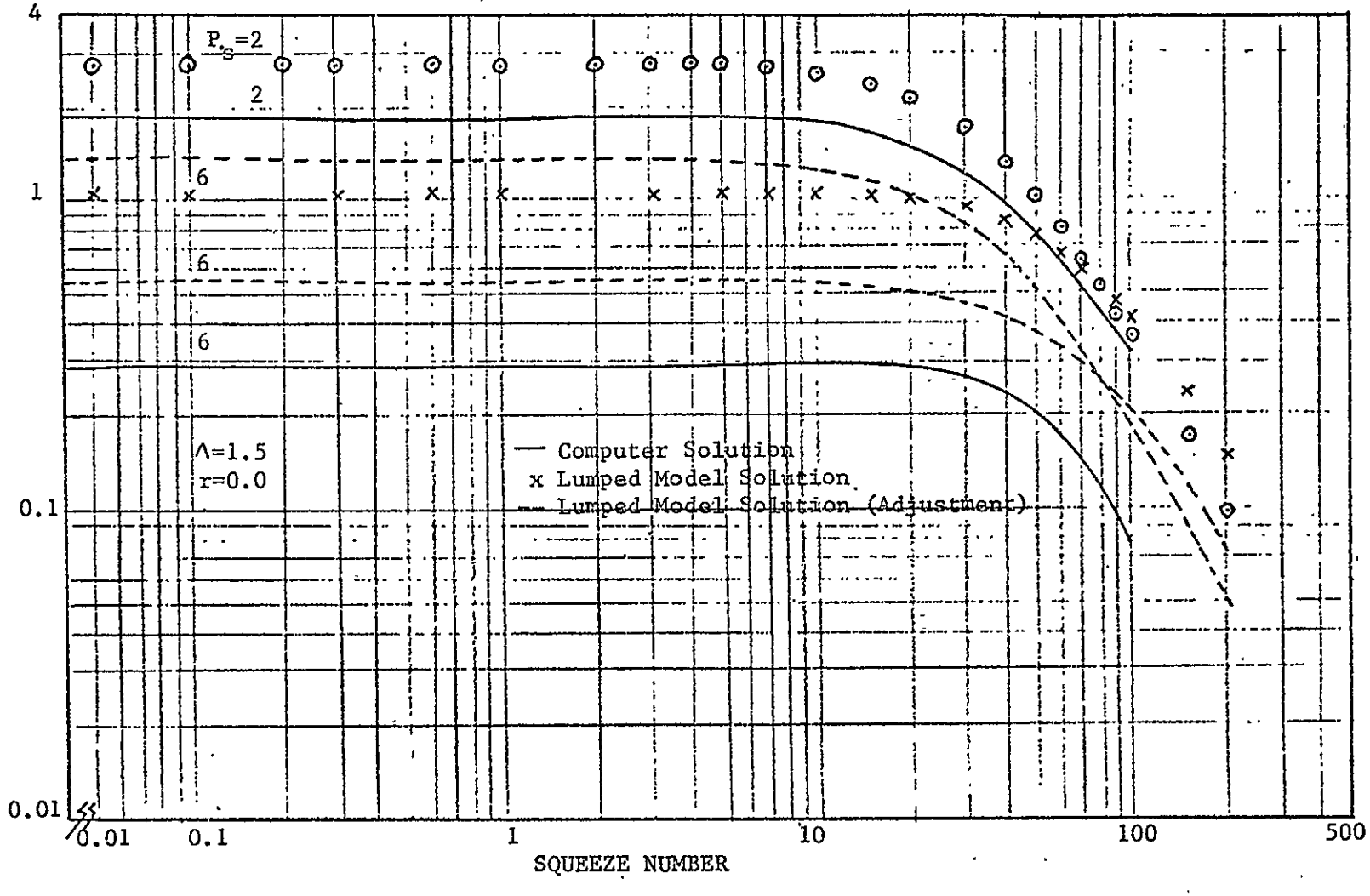

Figure 25. Square Bearing-Dimensionless Damping versus Squeeze Number (Λ= 5 , r=0.6)

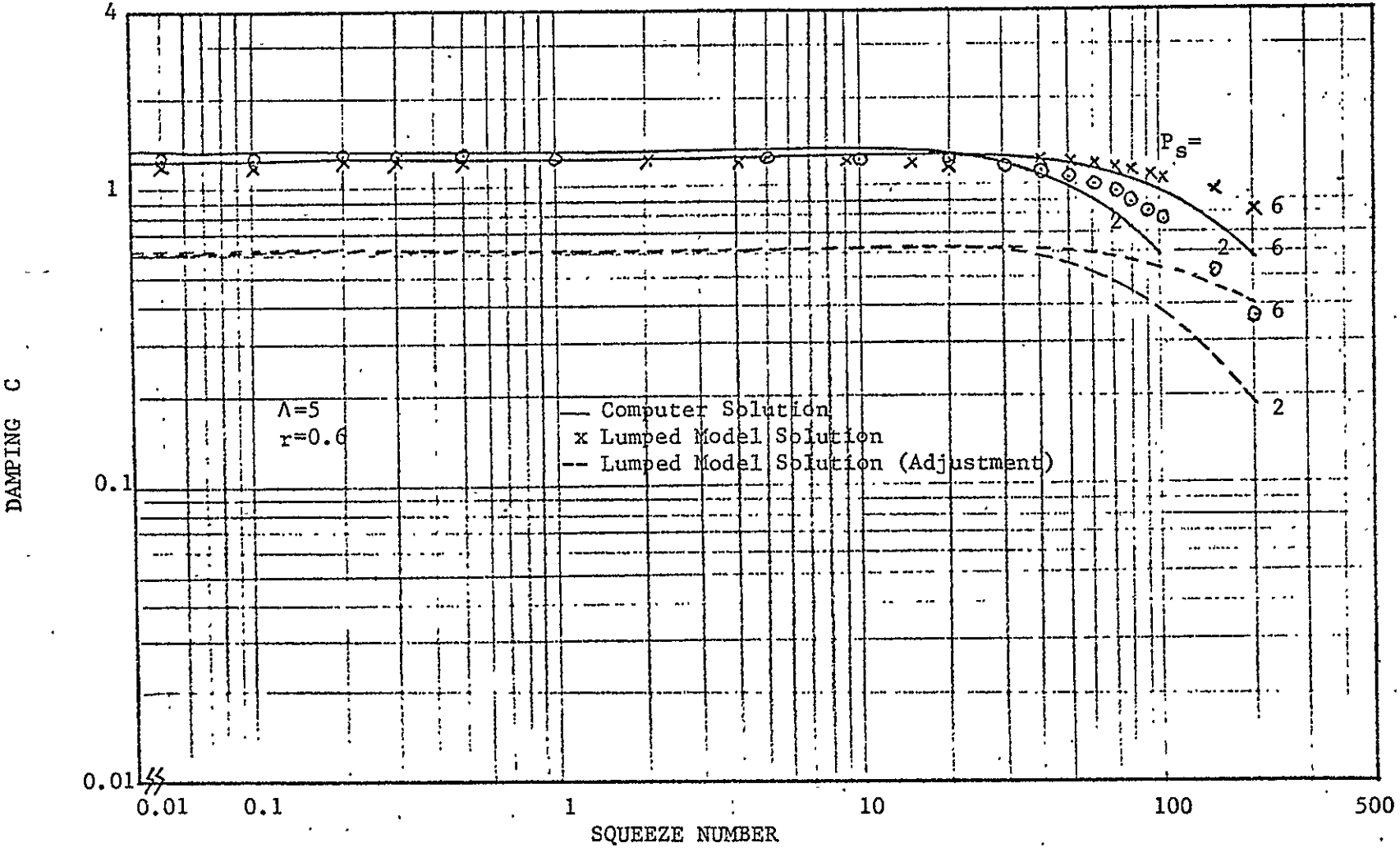

Figure 26 Square Bearing-Dimensionless Damping versus Squeeze number (Λ =5 , r=0.6)

CHAPTER VI

CONCLUSION

The dimensionless design parameters stiffness and damping obtained from the study of the strip bearing by lumped parameter methods are compared with those of Stiffler and Tapia [9] who used finite-difference methods. It is observed that the stiffness obtained from this study agrees well with computer solutions; however, the damping works well for the range of low restrictor coefficients only, $\Lambda \leq 10$, In discussing the effect of squeeze numbers on the stiffness and damping, the break frequencies for the lumped parameter damping appear to be realistic in spite of the inadequacy of the model.

The stiffness and damping obtained from the study of the square bearing by lumped parameter methods are compared with those of Stiffler and Smith [8] who used finite-difference methods. The stiffness obtained from this study is adequate when compared with computer solutions; however, the lumped model damping results offer poor agreement. If the damping from lumped parameter solution is adjusted according to Sadd and Stiffler's work on pure squeeze films [10], the results are improved but remain insufficient for predicting performance. On the study of the effect of squeeze number on the stiffness and damping, the break frequencies can be predicted well in spite of the inadequacy of the lumped model.

Since the lumped parameter model is an approximate technique to study the performance of the bearing, it is not surprising that the results differ from the computer solution. The corresponding film

volumes of the strip and square bearing are comparable in this study; so the lumped model displays no difference between a strip and a square, contrary to known results for pure squeeze films. This is one of the reason why much difference exists for the damping of the square bearing compared with computer solution. Because the prediction of the break frequencies for the lumped damping agrees well with computer solution, it can be concluded that the compressibility effect of the bearing film is well described by the lumped model, but the volume effect of the bearing film directly affects the accuracy of the lumped model. This suggests a starting point in future attempts to improve the lumped models for predicting bearing performance.

Regardless, the lumped model predicts the stiffness performances of both the strip and square bearing. Stiffness remains the single most important parameter in the design of rotor-bearing systems.

APPENDIX

TABLES FOR DIMENSIONLESS AVERAGE PRESSURE DOWNSTREAM OF INLET P_{ro} VERSUS RESTRICTOR COEFFICIENT Λ

TABLE 1

P_{ro} versus Λ for P_s=1.5

Λ	P_{ro}	Λ	P_{ro}	Λ	P_{ro}
30.0	1.49821271	3.0	1.39086568	1.1	1.22797903
25.0	1.49743451	2.9	1.38608333	1.0	1.21224958
20.0	1.49601475	2.8	1.38102095	0.9	1.19626465
15.0	1.49300268	2.7	1.37565945	0.8	1.17926772
13.0	1.49076996	2.6	1.36997833	0.7	1.16120100
10.0	1.48478685	2.5	1.36395567	0.6	1.14200700
9.5	1.48325201	2.4	1.35756799	0.5	1.13628988
9.0	1.48147882	2.3	1.35079020	0.4	1.11037100
8.5	1.47941673	2.2	1.34359550	0.3	1.08383246
8.0	1.47700148	2.1	1.33595521	0.2	1.05662759
7.5	1.47415061	2.0	1.32783875	0.1	1.02870352
7.0	1.47075716	1.9	1.31921364	0.09	1.02586931
6.5	1.46668082	1.8	1.31004522	0.08	1.02302725
6.0	1.46173548	1.7	1.30029668	0.07	1.02017727
5.5	1.45567120	1.6	1.28992908	0.06	1.01731930
5.0	1.44814827	1.5	1.27890107	0.05	1.01745329
4.5	1.43869943	1.4	1.26716911		
4.0	1.42667468	1.3	1.25468729		
3.5	1.41116081	1.2	1.24140742		

TABLE 2

P_{ro} versus Λ for P_s=2.0

Λ	P_{ro}	Λ	P_{ro}	Λ	P_{ro}
30.0	1.99566531	3.0	1.75674842	1.1	1.43055740
25.0	1.99378314	2.0	1.74677559	1.0	1.40156275
20.0	1.99075733	2.8	1.73626088	0.9	1.37082749
15.0	1.98312290	2.7	1.72516999	0.8	1.33825096
13.0	1.97778900	2.6	1.71346631	0.7	1.30373068
10.0	1.96361072	2.5	1.70111082	0.6	1.26716417
9.5	1.95999964	2.4	1.68806182	0.5	1.22845150
9.0	1.95584057	2.3	1.67427489	0.4	1.18915376
8.5	1.95102074	2.2	1.65970261	0.3	1.14479911
8.0	1.94539802	2.1	1.64429452	0.2	1.09865524
7.5	1.93879165	2.0	1.62799679	0.1	1.05048639
7.0	1.93096961	1.9	1.61075221	0.09	1.04554746
6.5	1.92163123	1.8	1.59249983	0.08	1.04058509
6.0	1.91038294	1.7	1.57317490	0.07	1.03559894
5.5	1.89670441	1.6	1.55270870	0.06	1.03058867
5.0	1.87990072	1.5	1.53102834	0.05	1.02555392
4.5	1.85903477	1.4	1.50805668		
4.0	1.83283118	1.3	1.48371223		
3.5	1.79954054	1.2	1.45790917		

TABLE 3

P_{ro} versus Λ for P_s=4.0

Λ	P_{ro}	Λ	P_{ro}	Λ	P_{ro}
30.0	3.98647532	3.0	3.28185204	1.1	2.34942020
25.0	3.98061584	2.9	3.25340634	1.0	2.26446465
20.0	3.96997054	2.8	3.22344931	0.9	2.17378415
15.0	3.94757229	2.7	3.19188359	0.8	2.07670250
13.0	3.93112689	2.6	3.15860465	0.7	1.97448896
10.0	3.88767972	2.5	3.12349993	0.6	1.86668690
9.5	3.87667309	2.4	3.08644813	0.5	1.75226519
9.0	3.86402442	2.3	3.04731832	0.4	1.62983025
8.5	3.84940305	2.2	3.00596910	0.3	1.49741777
8.0	3.83239442	2.1	2.96224735	0.2	1.35209960
7.5	3.81247442	2.0	2.91598718	0.1	1.18915376
7.0	3.78892463	1.9	2.86700832	0.09	1.17161342
6.5	3.76103487	1.8	2.81511469	0.08	1.15380645
6.0	3.72753779	1.7	2.76009242	0.07	1.13572033
5.5	3.68701782	1.6	2.70170777	0.06	1.11734149
5.0	3.63753356	1.5	2.63977452	0.05	1.09865524
4.5	3.57648709	1.4	2.57380115		
4.0	2.50036569	1.3	2.50368741		
3.5	3.40436783	1.2	2.42902044		

TABLE 4

P_{ro} versus Λ for P_s=6.0

Λ	P_{ro}	Λ	P_{ro}	Λ	P_{ro}
30.0	5.97818805	3.0	4.85050528	1.1	3.35083261
25.0	5.96874159	2.9	4.80510675	1.0	3.21184389
20.0	5.95158483	2.8	4.75729023	0.9	3.06353634
15.0	5.91550730	2.7	4.70689739	0.8	2.90750063
13.0	5.88903580	2.6	4.65375768	0.7	2.74260186
10.0	5.81916754	2.5	4.59768678	0.6	2.56713263
9.5	5.80148207	2.4	4.53848518	0.5	2.37875492
9.0	5.78116498	2.3	4.47593656	0.4	2.17411590
8.5	5.75768803	2.2	4.40980585	0.3	1.94809778
8.0	5.73038937	2.1	4.33983717	0.2	1.69215542
7.5	5.69843286	2.0	4.26575101	0.1	1.38985430
7.0	5.66075303	1.9	4.18724149	0.09	1.35592238
6.5	5.61597981	1.8	4.10397259	0.08	1.32111922
6.0	5.56233483	1.7	4.01557400	0.07	1.28537407
5.5	5.49748709	1.6	3.92163593	0.06	1.24860602
5.0	5.41835022	1.5	3.82170298	0.05	1.21072189
4.5	5.32079442	1.4	3.71526662		
4.0	5.19923231	1.3	3.60175480		
3.5	5.04601154	1.2	3.48052188		

TABLE 5

P_{ro} versus Λ for P_s =10.0

Λ	P_{ro}	Λ	P_{ro}	Λ	P_{ro}
30.0	9.96230993	3.0	8.02071861	1.1	5.42728355
25.0	9.94598984	2.9	7.94762822	1.0	5.18463272
20.0	9.91635353	2.8	7.86036927	0.9	4.92872952
15.0	9.85405193	2.7	7.77366594	0.8	4.65879094
13.0	9.80835372	2.6	7.68222058	0.7	4.37221815
10.0	9.68779554	2.5	7.58571070	0.6	4.06549504
9.5	9.65729118	2.4	7.48378688	0.5	3.73365882
9.0	9.62225356	2.3	7.37606757	0.4	3.36929763
8.5	9.58177395	2.2	7.26213835	0.3	2.96042648
8.0	9.53471429	2.1	7.14154576	0.2	2.48517268
7.5	9.47963733	2.0	7.01379247	0.1	1.89421267
7.0	9.41471222	1.9	6.87833134	0.09	1.82461982
6.5	9.33758552	1.8	6.73455792	0.08	1.75226520
6.0	9.24520336	1.7	6.58180171	0.07	1.67679133
5.5	9.13356413	1.6	6.41931492	0.06	1.59775623
5.0	8.99736908	1.5	6.24625905	0.05	1.51460253
4.5	8.82952800	1.4	6.06168748		
4.0	8.62044192	1.3	5.86452363		
3.5	8.35694816	1.2	5.65353259		

REFERENCES

1. Licht, L., Fuller, D. D., and Sternlicht, B. "Self-Excited Vibrations of an Air-Lubricated Thrust Bearing," Trans. ASME, Vol. 80, Feb. 1958, pp. 411-414.

2. Richardson, H. H., "Static and Dynamic Characteristics of Compensated Gas Bearings," Trans. ASME, Vol. 80, Oct. 1958, pp. 1503-1509.

3. Licht, L., and Elrod, H., "A Study of the Stability of Externally Pressurized Gas Bearings," Journal of Applied Mechanics, Vol. 27, Trans. ASME, Series E, Vol. 82, 1960, pp. 250-258.

4. Stiffler, A. K., "Analysis of the Stiffness and Damping of an Inherently Compensated, Multiple-Inlet, Circular Thrust Bearing," Journal of Lubrication Technology, Trans. ASME, Series F, Vol. 96, N.3, July 1974, pp. 379-432.

5. Mullan, P. J., and Richardson, H. H., "Plane Vibration of the Inherently Compensated Gas Journal Bearing; Analysis and Comparison with Experiment," Journal of Basic Engineering, Trans. ASME. Series D, Vol. 7, 1964, pp. 277-287.

6. Lund, J. W., "The Hydrostatic Gas Journal Bearing with Journal Rotation and Vibration," Journal of Basic Engineering, Trans. ASME, Series D, Vol. 86, June 1964, pp. 328-336.

7. Lund, J. W., "A Theoretical Analysis of Whirl Instability and Pneumatic Hammer for a Rigid Rotor in Pressurized Gas Journal Bearing," Journal of Lubrication Technology, Trans. ASME, Series F. Vol. 89, 1967, pp. 154-166.

8. Stiffler, A. K., and Smith, D. M., "Dynamic Characteristics of an Inherently Compensated, Square, Gas Film Bearing," Journal of Lubrication Technology, Trans. ASME, Series F, Vol, 97, Jan. 1975, pp. 52-62.

9. Stiffler, A. K., and Tapia, R. R. The Effect of Amplitude on the Dynamic Characteristics of Inherently Compensated Gas Thrust Bearings," MSSU-EIRS-ME.76.1.

10. Sadd, M. H., and Stiffler, A. K., "Squeeze Film Dampers: Amplitude Effects at Low Squeeze Numbers," Journal of Engineering for Industry, Trans. ASME, Series B, Vol. 97, Nov. 1975, pp. 1366-1370.

11. Salbu, E. O. J., "Compressible Square Films and Squeeze Bearings," Journal of Basic Engineering, Trans. ASME, Series D. Vol. 86, 1964, pp. 355-364.

12. Constantinescu, V. N., Gas Lubrication, Translated Scripts Technica, Inc. New York: The American Society of Mechanical Engineers, 1964

13. Fleming, D. P. Cunningham, R. E., and Anderson, W. J., Stability Analysis for Unloaded Externally Pressurized Gas-Lubricated Bearings with Journal Rotation, NASA TN D-2934, Dec., 1968.

14. Pinkus, Oscar, and Sternlicht, Beno. Theory of Hydrodynamic Lubrication; New York: McGraw-Hill, 1961, pp. 196-200.

PART II:

VELOCITY PROFILES NEAR THE INLET OF THE INHERENTLY COMPENSATED BEARING

INTRODUCTION

One of the main difficulties in the use of analytical or computer solutions of inherently compensated gas bearings to predict dynamic performance is the apparent disagreement with experimental results [1][2]. In the view of this writer the crux of the problem is that the solutions for capacity, stiffness, and damping depend upon the discharge coefficient for the inherent orifice as the flow enters the bearing surface from the inlet hole. Limited experimental values for the discharge coefficient can be found [3], but they are not entirely satisfactory. Furthermore, there is no knowledge of the dependence of discharge coefficients on the frequency of the disturbance.

The purpose of this initial study on inherently compensated discharge coefficients is to determine experimentally the velocity profiles near the feed region of the inlet. Eventually dynamic studies would contribute the main effort. This work is only in the beginning stage, and a brief outline of the progress to date follows.

EXPERIMENTAL PROCEDURE

The characteristic film thickness of gas bearings is at most a few thousandths of an inch. Thus, flow visualization studies require a scaling based upon the Reynolds number [4]. A plexiglass model of the feed inlet was constructed with a slot gap adjustable from 1/8 in. to 3/8 in. and a width of 2 in., Figure 1. A water circulating system was built into the set up with a pump capacity sufficient to achieve Reynolds numbers on the order of 6000.

Birefringence Effect

For many years photoelasticity has been a very useful method for experimental stress analysis in solids. This method is based on the fact that certain substances become temporarily doubly refracting when they are stressed. An analogous phenomenon in liquids is known as flow birefringence. The photoviscous analysis of the birefringence patterns to determine velocity distributions in steady, laminar flow is widely known [5].

When an aqueous solution of commercial organic dye, Milling Yellow NG5, is caused to flow through a transparent viewing channel and subjected to polarized light, the fluid becomes double refracting and produces visible interference patterns which are seen as alternating dark and light bands. The dark bands, isochromatics, represent the loci of points where the magnitude of the shearing stresses are the same. The velocity profiles are then obtained from integration of the shear stress profiles.

The optical system used in the experiments was readily available in the experimental stress lab at Mississippi State University. The basic system consists of a sodium-vapor light source, two collimating lenses, two polarizing plates, two quarter wave plates, and an optical bench.

Particulate Effect

An alternate source of flow visualization consisted of particles suspended in water. Motion of these particles was recorded in the following manner. A collimated light beam with a width of approximately 1/4 of an inch was projected vertically through the flow from above, Figure 1. When viewed from a horizontal position, the motion of these particles was visible in this plane of light. Photographic records of particle motion were made.

Two particulates were used: (1) small hollow glass spheres approximately .001 inch in size, (2) a certain dishwater detergent which apparently has

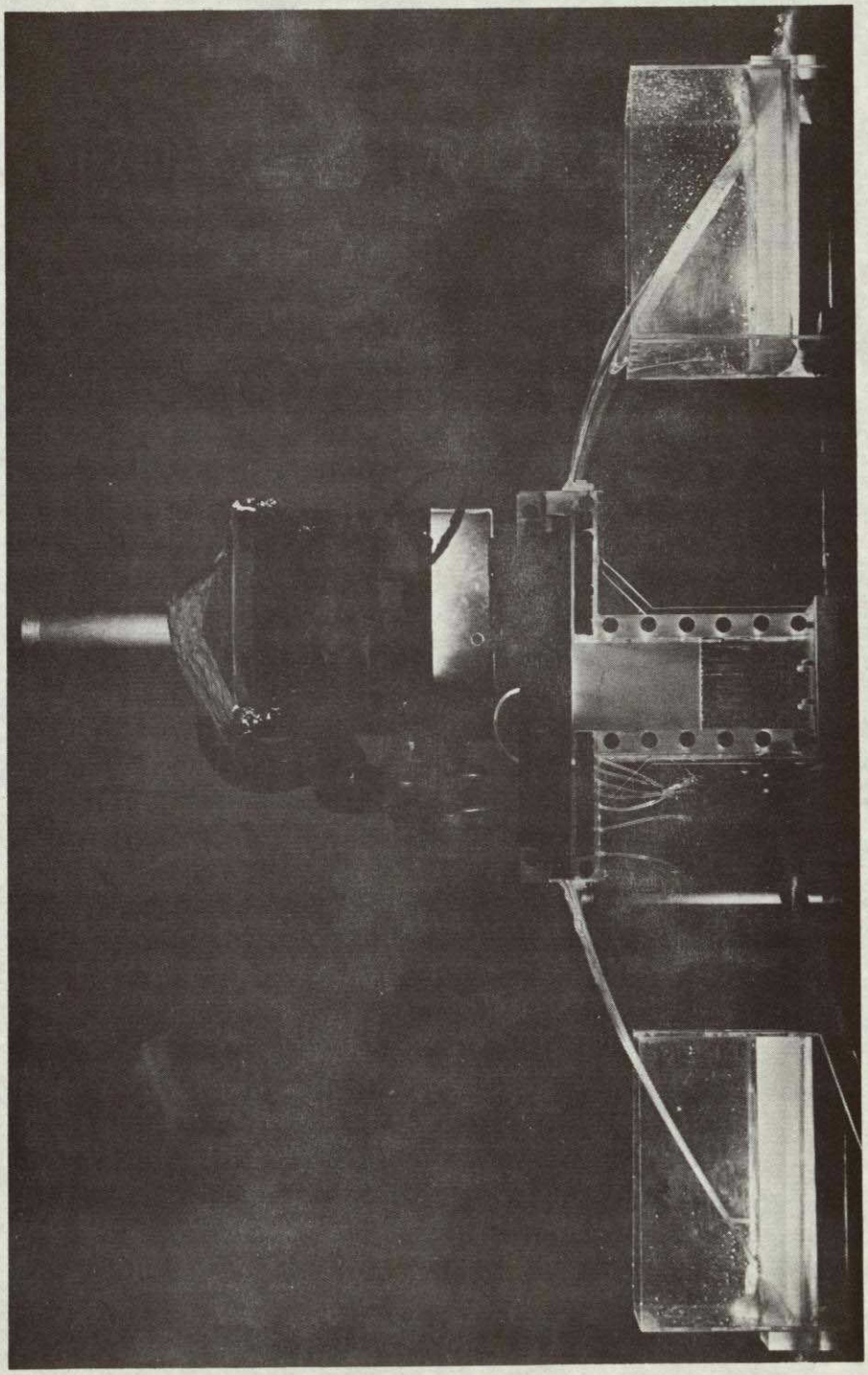

FIG. 1. Visualization of Flow Over a Corner.

suspended extremely small abrasives. Trial and error procedures lead to the use of 1/100 gram per gallon of the former and 2 drops per gallon of the latter.

Hot Wire Anemometer

In place of the aqueous solutions above a direct attack on the velocity profiles can be obtained from hot wire measurements using air. This procedure is so standard that no futher summary is given. The biggest drawback to the use of a hot wire is the subsequent interference of the flow field by the probe itself--an unknown effect.

RESULTS

Birefringence Effect

The original plan was to make use of a birefringent fluid since the flow field is unobstructed and the field can be obtained throughout with one test run. Unfortunately the literature on birefringence was not explicit in explaining several difficulties when working with Milling Yellow. This approach was abandoned for the following reasons:

(1) Very little is known about the rheological properties of Milling Yellow, particularly the relationship of birefringence with the shear stress which is non-Newtonian;

(2) concentrations as narrow as 1 1/4 - 1 1/2 per cent are necessary and these concentrations show a highly nonlinear relationship with the amount of birefringence;

(3) birefringence is very sensitive to temperature with as little as one degree variation introducing a sizable error. Pumping losses can account for several degrees change in the solution temperature;

(4) the planned dynamic studies would undoubtably result in a total effort to obtain the rheological properties of the Milling Yellow and very little realizable data on the fluid mechanics of the problem.

Particulate Effect

After a concerted effort with the particulate solution approach to flow visualization this phase was abandoned for the following reasons:

(1) Although the flow patterns were observable to the naked eye, it proved to be very difficult to photograph the patterns, and professional photographers at the University offered little hope;

(2) the experience also suggested that the photographs, if obtainable, could be used for a qualitative picture of the flow field but of marginal value determining the velocity profiles.

Hot Wire Anemometer

The hot wire anemometer appears to be the only logical choice for establishing the flow field accurately. A test run was conducted by simply inserting a miniature probe into the slot opening and tracing the flow field from the leading edge of the step. Pressure taps were placed at several stations from the leading edge so that the discharge coefficient could be found directly. Tenative results were compared with the analytical work of Hagerup [4]. Some of the findings are as follows.

A well defined separation bubble exists and its length is approximately two film thicknesses from the step edge, Figure 2. This value corresponds to a theoretical Reynolds number of 500, Figure 3. The calculated value for the test run was approximately 3600 based upon an average exit velocity.

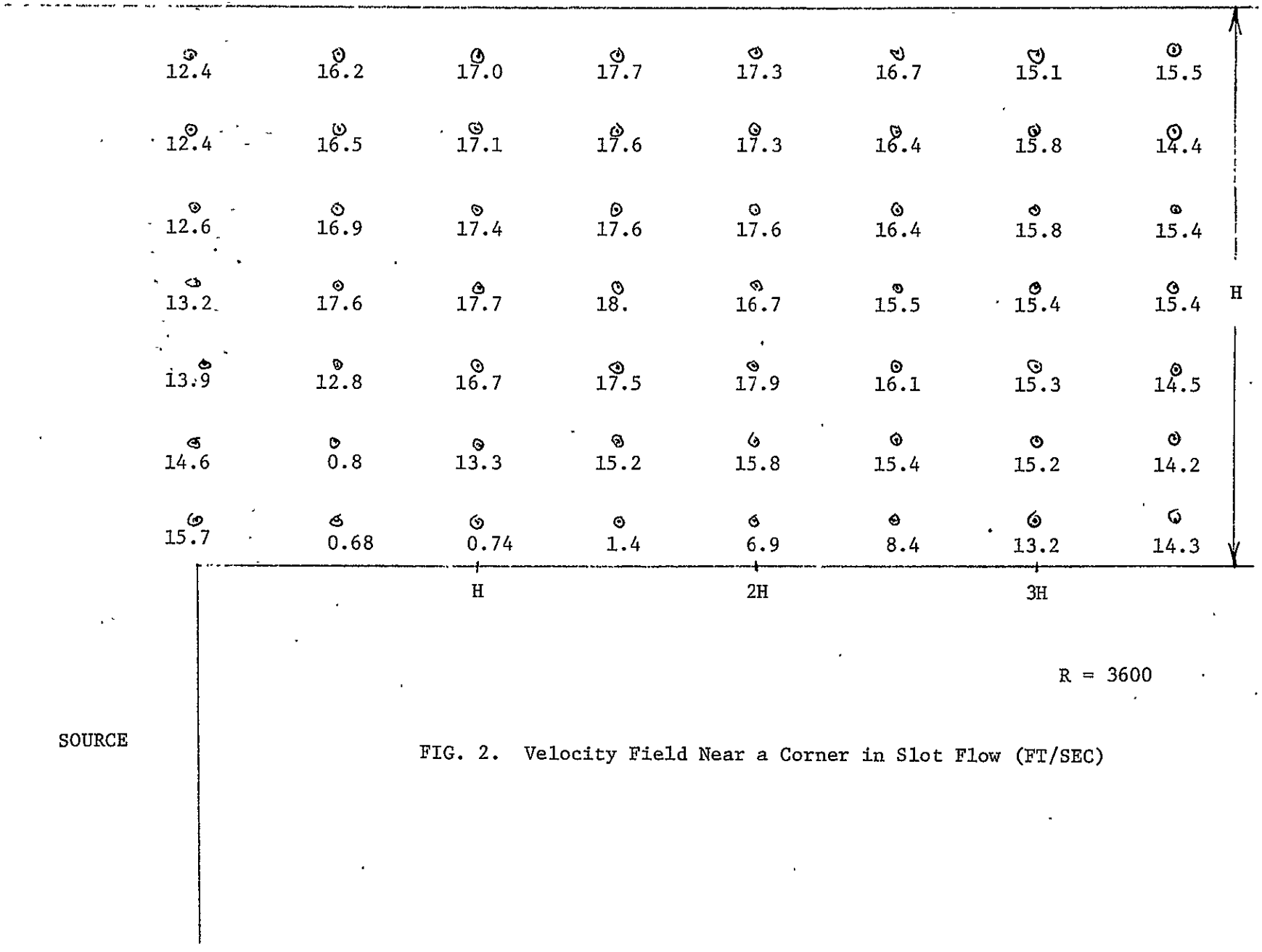

FIG. 2. Velocity Field Near a Corner in Slot Flow (FT/SEC)

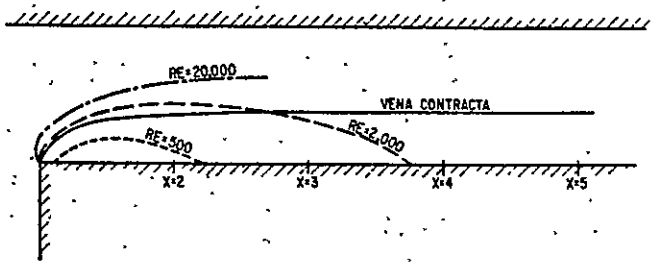

Calculated separation streamlines for several Reynolds numbers

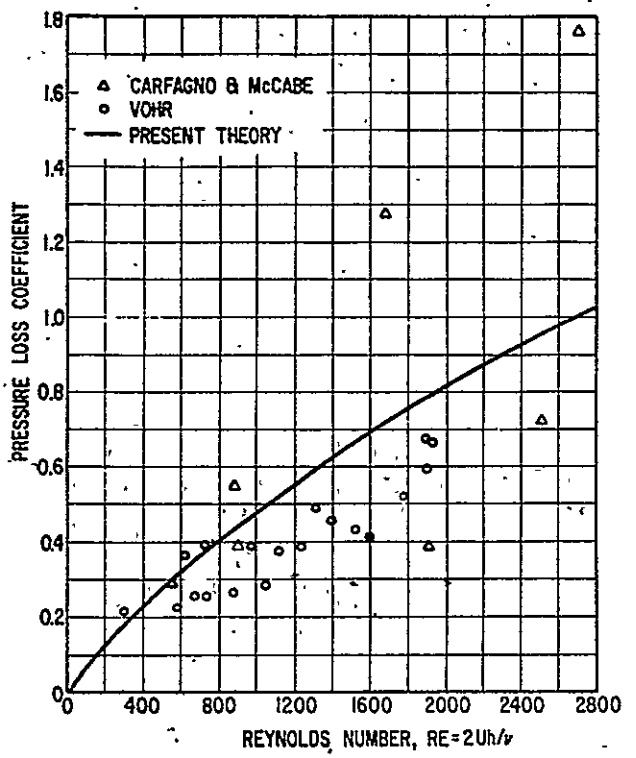

Inherent restrictor pressure loss coefficient as function of Reynolds number

FIG. 3. Theoretical Results from Hagerup [4]

Hagerup [4] defines the loss coefficient as

$$\Delta p = \frac{1}{2} k\rho U^2$$

which has a corresponding discharge coefficient

$$c_d = [\frac{1}{1+k}]^{1/2}.$$

The theoretical discharge coefficient for R = 500 is $c_d = 0.88$. The calculated values from the experiment were $c_d = 0.88$ for a Reynolds number range 2400-4000.

The results would agree with the theoretical calculations provided the measured Reynolds number was smaller by a factor of 6-8. All velocity measurements were referenced to a "Magnehelic" pressure gauge with a direct read out in inches of water. There is insufficient data to draw meaningful conclusions from the experiments. It is possible that the probe itself is interferring with the flow pattern. Future experiments will be conducted with a larger model of the inlet corner.

REFERENCES

1. Pink, E. G., "Investigations into Design Methods for Externally Pressurized Gas Journal Bearings", 6th Inter. Gas Bearing Sym., March 27-29, 1974, Univ. of Southampton.

2. Cunningham, R. E., et.al., "Design of a Squeeze Film Damper for a Multi-Mass Flexible Rotor", J. of Eng. for Ind., ASME Trans., Nov. 1975, p. 1383-1390.

3. Vohr, J. H., "An Experimental Study of Flow Phenomena in the Feeding Region of an Externally Pressurized Gas Bearing", MTI-65TR47, Mechanical Technology, Inc., 1965.

4. Hagerup, H. J., "On the Fluid Mechanics of the Inherent Restrictor", ASME paper 74-FE-26, 1974.

5. Wayland, H., "Streaming Birefringence as a Rheological Research Tool", J. of Polymer Science, Part C, No. 5, 1964, p. 11-36.